The age and structure of dikes along the tectonic contact of the Ivrea-Verbano and Strona-Ceneri Zones (southern Alps, Northern Italy, Switzerland)

Autor(en): **Mulch, Andreas / Rosenau, Matthias / Dörr, Wolfgang**

Objekttyp: **Article**

Zeitschrift: **Schweizerische mineralogische und petrographische Mitteilungen = Bulletin suisse de minéralogie et pétrographie**

Band (Jahr): **82 (2002)**

Heft 1

PDF erstellt am: **22.09.2024**

Persistenter Link: https://doi.org/10.5169/seals-62352

SCHWEIZ. MINERAL. PETROGR. MITT. 82, 55–76, 2002

The age and structure of dikes along the tectonic contact of the Ivrea-Verbano and Strona-Ceneri Zones (southern Alps, Northern Italy, Switzerland)

by *Andreas Mulch*[1*], *Matthias Rosenau*[1#], *Wolfgang Dörr*[1] and *Mark R. Handy*[1§]

Abstract

A 2–3 km wide shear zone, the Cossato-Mergozzo-Brissago Line (CMB Line), forms the contact between two subvertically dipping basement units of the southern Alpine continental crust: the Ivrea-Verbano Zone (IVZ) and Strona-Ceneri Zone (SCZ). The CMB Line is characterized by a steeply dipping mylonitic foliation with variably oriented stretching lineations and syn-mylonitic mafic and felsic dikes. Syn-mylonitic intrusion of these dikes is documented by mutually crosscutting dikes and host mylonites and by leucocratic tension gashes within the mafic dikes that display the same sense-of-shear as the surrounding mylonites. Structural analysis of the northeastern end of the IVZ demonstrates that, similar to other segments of the CMB Line, the CMB mylonites are locally overprinted by a younger amphibolite to greenschist facies mylonite zone, the Pogallo Line. As the CMB- and Pogallo Lines affected the southern Alpine crust at different times, dating them clarifies their contrasting roles in the evolution of the southern Alpine continental crust. U–Pb geochronology reveals that intrusion of the investigated syn-mylonitic dikes and hence, mylonitization along the CMB Line, occurred in Early Permian time (275–285 Ma). Metamorphic titanite within the same dikes formed at 173 ± 4 Ma supposedly as a result of discontinuous retrograde metamorphic reactions associated with crustal attenuation that was localized along the Pogallo Line. Pogallo mylonitization therefore clearly postdates Early Permian CMB activity.

Structural and U–Pb zircon data support models of the CMB Line as the subhorizontal part of an Early Permian transcurrent shear zone that accommodated oblique-slip faulting and basin formation in the upper crust, and ductile thinning and exhumation of the lower crust. The CMB mylonite belt linked Early Permian magmatism in different levels of the crust by serving as a conduit for the ascent of melts from the underplated Mafic Complex in the Ivrea-Verbano Zone into intermediate crustal levels that are currently exposed along the contact between the Ivrea-Verbano and the Strona-Ceneri Zones. In the proposed model for the IVZ these melts subsequently induced partial melting of upper amphibolite facies metasedimentary rocks making up the CMB mylonites.

Keywords: geochronology, geochemistry, Ivrea Zone, shear zone, melts.

Introduction

Crustal-scale mylonitic shear zones play an important role in the syn- to post-orogenic evolution of the crust. However, the interpretation and correlation of tectonic processes acting in different crustal levels is often obscured by the lack of coherent basement units exposing such crustal levels and their imprecisely known temporal and kinematic history. The Ivrea-Verbano Zone (northern Italy and Switzerland) offers a unique field area for the study of magmatic and deformational processes in intermediate and lower crustal levels. There, Tertiary thrusting and folding exposed magmatically underplated lower continental crust (ZINGG et al., 1990; HANDY and ZINGG, 1991; SCHMID, 1993). This study focuses on the so-called Cossato-Mergozzo-Brissago Line (CMB Line), a 2–3 km broad, upper amphibolite facies mylonite zone within the southern Alpine base-

[1] Institut für Geowissenschaften, Justus-Liebig Universität Giessen, Senckenbergstrasse 3, D-35390 Giessen, Germany.
Present addresses:
[*] Institut de Minéralogie et Géochimie, Université de Lausanne, BFSH2, CH-1015 Lausanne, Switzerland.
<andreas.mulch@img.unil.ch>
[#] GeoForschungsZentrum Potsdam (GFZ), Telegrafenberg, D-14473 Potsdam, Germany.
[§] Endogene Geologie, Freie Universität Berlin, Malteser Strasse 74-100, D-12249 Berlin, Germany.

ment (BORIANI et al., 1990). The CMB Line is spatially associated with numerous mafic and felsic dikes and stocks (in the local literature often referred to as "Appinites"; BORIANI et al., 1974) and forms the tectonic contact between the Ivrea-Verbano (IVZ) and Strona-Ceneri (SCZ) Zones, southern Alps (Fig. 1). These dikes are important time markers for constraining the tectonic history of the southern Alpine basement units.

A continuing debate centers on the extent and location of Early Permian versus Early Mesozoic extension in the southern Alpine basement (e.g. TRÜMPY, 1992; SCHUMACHER et al., 1997). By dating the intrusive rocks along the CMB Line, we intend to test whether one or both of these extensional events were associated with mafic underplating. Specifically, we seek to determine whether Early Permian extensional tectonics were spatially and temporally distinct from Early Mesozoic rifting of the Apulian continental margin, or whether one protracted extensional event, lasting from Early Permian to Early Jurassic time, effected exhumation of the southern Alpine crust.

New TIMS U–Pb data obtained for this study from hornblende-dioritic and muscovite granite dikes along the CMB Line confirm that post-Variscan, Early Permian transtension of the southern Alpine continental crust was temporally distinct from subsequent Early Mesozoic rifting. Mutually crosscutting relationships between the different dikes along the CMB Line indicate that these intrusives are cogenetic (ZURBRIGGEN, 1996; MULCH, 1999). Whole rock geochemical data favor the interpretation that the different dikes are genetically linked and support a structural model in which melt ascent was fostered by CMB mylonitization.

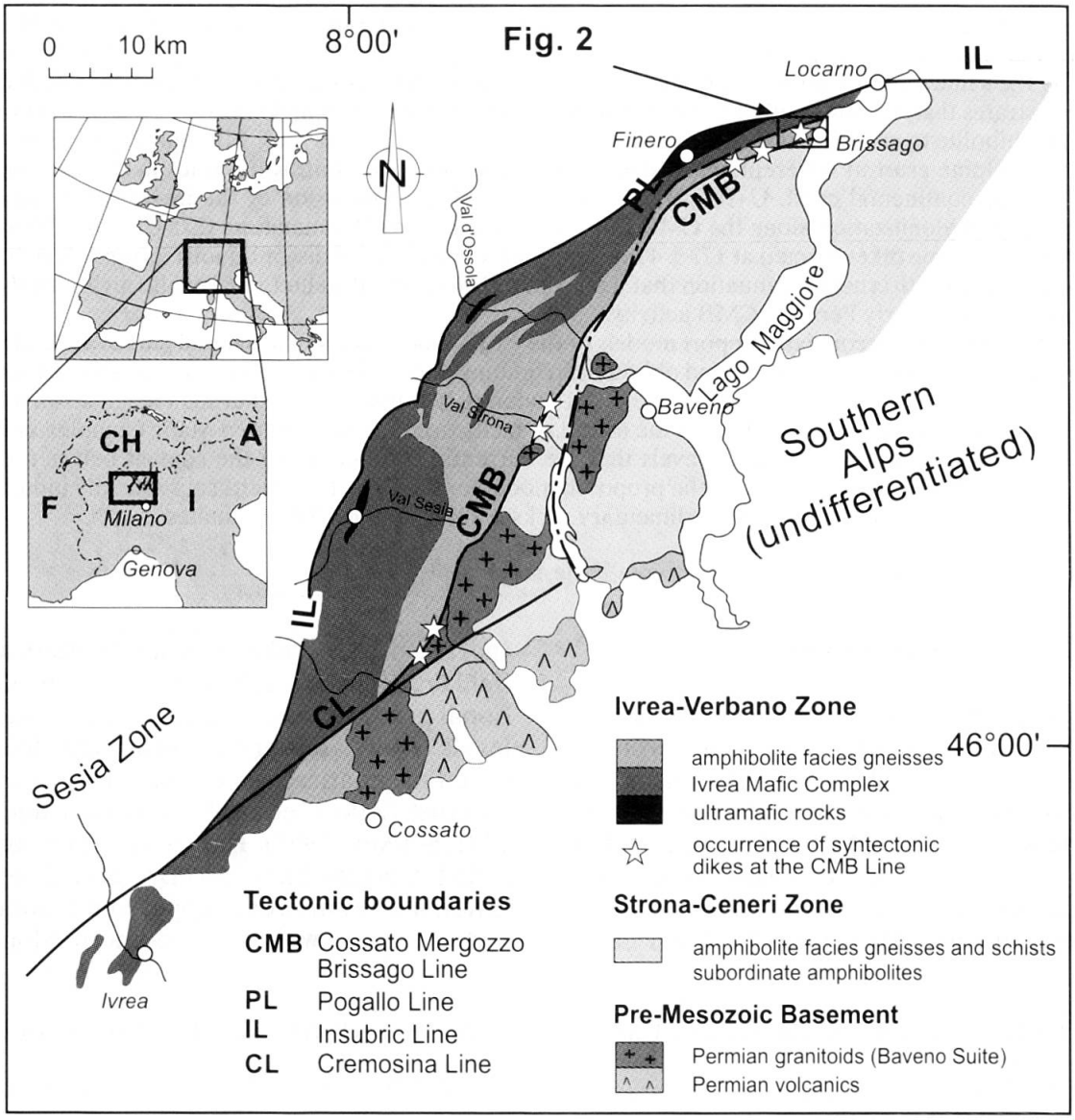

Fig. 1 Sketch map of the western part of the southern Alpine basement units modified from ZINGG et al. (1990). Framed area is shown in detail in Figure 2.

Geological setting of the CMB mylonites and dikes

The IVZ and SCZ represent parts of tilted Paleozoic basement that are separated from Alpine metamorphic units to the north by the Oligo-Miocene Insubric Line (Fig. 1, e.g. SCHMID et al., 1987). The basement exposed today in map view comprises a cross-section of thinned lower and intermediate pre-Alpine continental crust as it existed at the end of Early Jurassic rifting (ZINGG et al., 1990). Both the IVZ and SCZ underwent polyphase burial and exhumation during their Paleozoic evolution (synthesis in HANDY et al., 1999). The lower crustal mylonitic shear zones making up the CMB Line attenuated and partly exhumed the southern Alpine, intermediate to lower continental crust (e.g. HANDY et al., 1999). The CMB Line is therefore thought to be contiguous with oblique-slip faults bounding elongate transtensional basins (e.g. Collio basin; CASSINIS et al., 1995) and Early Permian shallow-level granitoid plutons in the upper crust (reconstructions of HANDY and ZINGG, 1991; HANDY et al., 1999). The broad spectrum of isotopic ages in the IVZ has often been interpreted to reflect repeated thermal and/or fluid activity related to superposed, crustal-scale tectonic events (e.g. von QUADT et al., 1993; GEBAUER, 1993; VAVRA et al., 1999). A swarm of elongate ENE–WSW striking hbl-dioritic to granitic dikes in the originally deep-seated northernmost segment of the southern Alpine basement coincides with the CMB Line. The pervasive mylonitic foliation of the CMB Line is presently subvertically oriented and is sub-parallel to older main foliations in the adjacent IVZ and SCZ, respectively, of Variscan and Ordovician ages (HANDY et al., 1999). In the Brissago area (Fig. 1), upper amphibolite facies conditions prevailed during CMB mylonitization as documented by local anatexis in the deformed mica-gneisses and the syn-kinematic qtz + pl + bt + sil + grt ± kfs ± ms assemblage.

It is important to note that the CMB Line is not the only mylonite belt in the southern Alpine basement. Locally the CMB mylonites are cross-cut and partly overprinted by the Pogallo mylonites (Figs. 1, 2, e.g. BORIANI and SACCHI, 1973) which themselves are truncated by mylonites and cataclasites related to the Oligo-Miocene Insubric Line (HANDY, 1987). During Early Mesozoic time the Pogallo Line was a low-angle normal fault zone that extensionally exhumed large parts of the intermediate to deep southern Alpine continental crust (HANDY et al., 1999 and references therein). The Pogallo mylonites overprint central and eastern parts of the CMB Line (Fig. 1). Neither the orientation of structures nor syn-mylonitic metamorphic conditions (in the northeastern IVZ) can be used to unequivocally discriminate between CMB- and Pogallo mylonites. In the study area, however, both foliations can be distinguished because of different overprinting relationships with respect to the investigated dikes.

Relative age and conditions of diking and deformation

The CMB Line is characterized by four different features. First, it is a zone of mylonitic shear within the southern Alpine basement. Second, it coincides with a gradational lithologic contact between the IVZ and SCZ. Third, it coincides with a swarm of hornblende dioritic to granitic dikes (Fig. 1). These dikes are best exposed at the northeastern end of the CMB Line near the town of Brissago (Fig. 2) where fresh exposures show mutually overprinting relationships of the dikes with the CMB mylonites. Fourth, the CMB Line is accompanied by localized partial melting in the mylonites. BORIANI et al. (1977, 1990) were the first to observe partial melts within the mylonitic host rock and to propose that CMB mylonitization took place under high-temperature conditions prior to the intrusion of the dike swarm. However, by mapping the overprinting relationships between the dikes and the deformation in the surrounding mylonites, ZURBRIGGEN (1996) and MULCH (1999) found that this composite dike swarm intruded during (rather than before) mylonitization in the country rock.

Most observations presented here are based on detailed mapping of stream bed outcrops that provide continuous sections across strike of the subvertically dipping CMB mylonites. In the area of investigation the common lithology within the CMB mylonites is a high-Al metapelite with sillimanite as the stable aluminosilicate polymorph, and subordinate marbles, metabasites and metaquartzites. Metamorphic conditions during the mylonitization are constrained by the presence of fibrous sillimanite on biotite-rich foliation surfaces and the incipient breakdown of primary muscovite. The occurrence of leucosomes in the vicinity of hornblende-dioritic dikes is consistent with uppermost amphibolite facies conditions during the intrusion of the dikes. These observations imply the reaction:

$$\text{muscovite} + \text{quartz} + \text{plagioclase} + \text{water} = \text{sillimanite} + \text{melt}.$$

At estimated pressures of about 4–6 kbar during mylonitization (see discussion in HANDY and

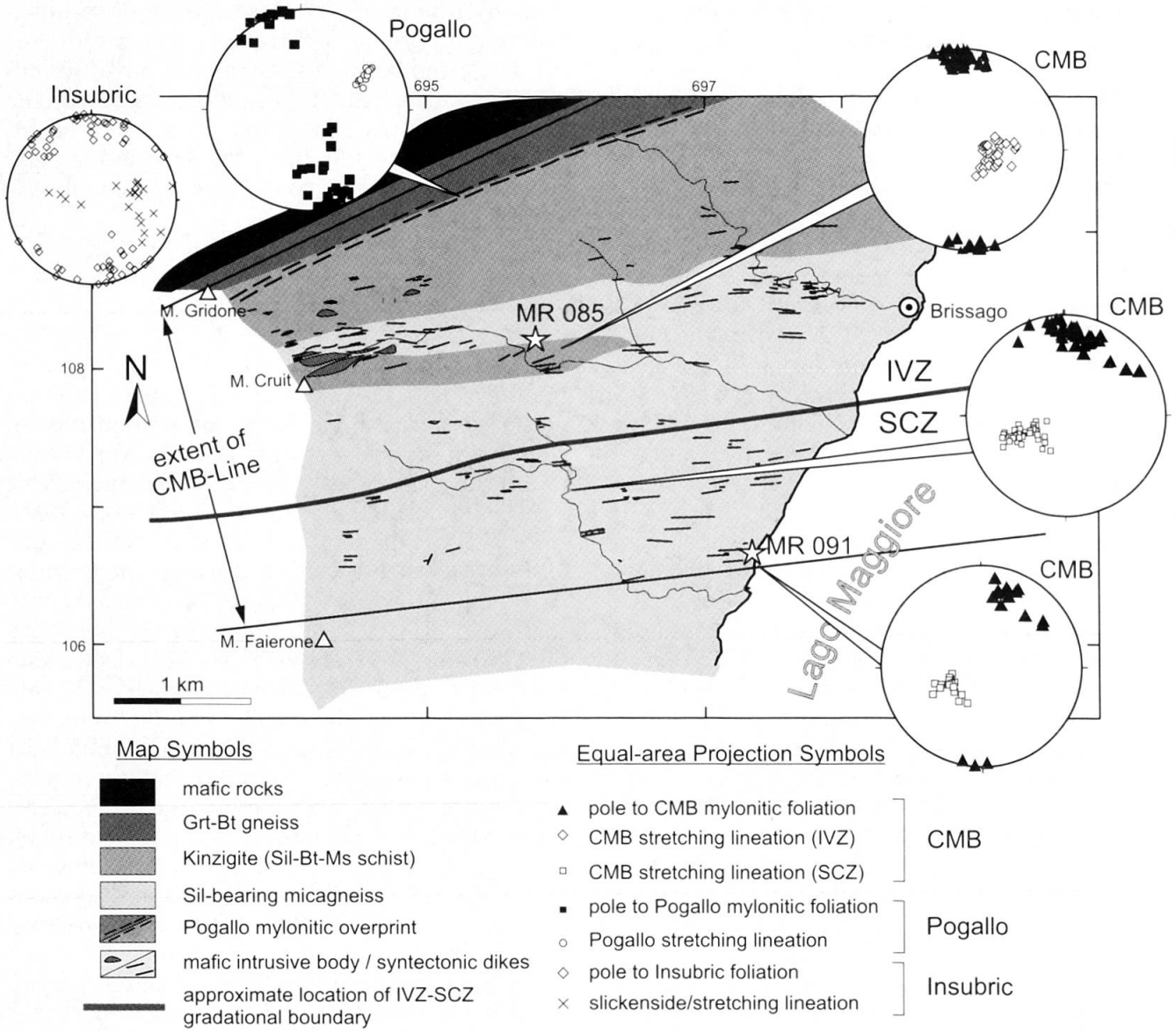

Fig. 2 Structural map of the Brissago segment of the CMB Line and the inferred contact of the IVZ and SCZ marked by a significant change in stretching lineations (after MULCH, 1999). Swiss topographic map grid coordinates are given for reference.

STREIT, 1999), this reaction is consistent with deformational temperatures of 600–650 °C (CLEMENS, 1984) in the CMB mylonites close to the hornblende-dioritic dikes. The CMB mylonites are inferred to have accommodated non-coaxial, oblique sinistral flow parallel to moderately eastward-dipping mineral stretching lineations in the IVZ (Fig. 2 and HANDY and STREIT, 1999). In the SCZ, CMB mineral stretching lineations are inferred to overprint an older lineation of unknown age (Fig. 2). The interpretation that the CMB dikes intruded during mylonitization is based on the observation that some dikes are undeformed and preserve primary magmatic features (e.g. chilled margins or magma mingling structures as shown in Fig. 3c), while other dikes in the same outcrop are sheared or asymmetrically boudinaged (Fig. 3a). The proximity of pre-, syn- and post-mylonitic dikes within a single outcrop therefore indicates that individual dikes intruded quickly and sporadically during a prolonged period of mylonitic flow (HANDY and STREIT, 1999).

Another argument for syntectonic diking is the presence of tension gashes and pull-apart structures filled with granitic rock within the hornblende-dioritic dikes. The right-stepping en-echélon geometry of these tension gashes indicates an overall sinistral sense of shear (criterion of RAMSAY and HUBER, 1983; Figs. 3 a, b). Leucosomes at the contact of the hornblende-dioritic dikes and the country rock (Fig. 3b) are interpreted as evidence of partial melting in response to heat advected by the dikes. The localization of these former partial melts within the necks of the

hornblende-dioritic dikes indicates that these dikes had acquired a fracture strength and therefore had crystallized during deformation. Evidence for localization of partial melts as dikes within the mylonites comes from ubiquitous garnet in granite and pegmatite dikes of the CMB dike swarm as described by ZURBRIGGEN (1996). The presence of significant modal garnet points to melting of a peraluminous source rather than fractionation of purely mantle-derived melts. Mingling of host rock-derived partial melts and hornblende-diorites led to the formation of isolated enclaves or 'schollen' of diorite within a tonalitic to locally granitic matrix (Fig. 3d). These enclave-bearing composite dikes are characteristic for the CMB dike swarm. As above, the schollen indicate that the mafic melt had crystallized and attained a strength sufficiently high to enable fracturing. We also observed dikes of hybrid composition, some lesser deformed varieties of which contained schlieren structures (Fig. 3c). Schlieren structures are diagnostic of low strength contrasts between compositionally different melts. We therefore interpret hybrid dike compositions and schlieren structures as evidence for melt mixing.

In contrast to these structures that result from CMB deformation (e.g. asymmetric boudinage in the presence of a granitic melt), Pogallo mylonitization postdates intrusion of the investigated dikes. Pogallo deformation resulted in the formation of blocky boudins of dioritic CMB dikes, highly sheared dike margins without syn-deformational melting in the host rock.

Previous isotopic constraints on the age of syntectonic dike intrusion

The numerous isotopic and geochronological investigations in the IVZ and SCZ published during the last 30 years (compilations in ZINGG et al., 1990; HUNZIKER et al., 1992; more recent U–Pb work in VAVRA et al., 1996) have enabled the documentation of Early Permian magmatism in three different levels of the southern Alpine continental crust: (1) 280–285 Ma volcanics in the Collio basins of the Bergamasca Alps (CASSINIS et al., 1995; SCHALTEGGER and BRACK, 1999), (2) shallow granitic plutons of the Baveno granitoid suite in the SCZ (275–280 Ma, e.g. BORIANI et al., 1988; PINARELLI et al., 1988; BORIANI et al., 1992), and (3) post-regional metamorphic gabbro-diorites of the Mafic Complex in the IVZ (ZINGG, 1983; 285 +7/–5 Ma of PIN, 1986).

VAVRA et al. (1996, 1999) reconstructed the zircon growth and recrystallization history in the IVZ during the Late Palaeozoic and Early Mesozoic with the SHRIMP method. They concluded that high-grade metamorphism associated with short-lived magmatism and anatexis in the IVZ at 299 ± 5 Ma was followed by the intrusion of the dioritic rim of the Ivrea Mafic Complex dated at 285 +7/–5 Ma (U–Pb zircon; PIN, 1986). These mafic intrusives therefore post-date earlier, late Carboniferous mafic rocks that triggered amphibolite to granulite facies regional metamorphism in the IVZ, but that preceded a local post regional-metamorphic temperature climax restricted to the rocks adjacent to the Mafic Complex in Val Sesia (for a detailed discussion see ZINGG, 1983 and HANDY et al., 1999). The minimum age of this local temperature climax corresponds to cooling through closure of monazite at about 273–275 Ma (KÖPPEL, 1974; HENK et al., 1997). Subsequent hydrothermal events at about 210–230 Ma strongly affected U–Pb and Sm–Nd isotopic mineral systems of the IVZ, as indicated by several geochronological investigations (e.g., STÄHLE et al., 1990; GEBAUER, 1993; von QUADT et al., 1993; OPPIZZI and SCHALTEGGER, 1998; VAVRA and SCHALTEGGER, 1999). The $^{40}Ar/^{39}Ar$ data of BORIANI and VILLA (1997) showed very complex trajectories in correlation diagrams for hornblendes from mafic dikes of the Brissago area, hindering the determination of a reliable, geologically meaningful age. However, they favored a lower limit for the crystallization age of the dikes at about 220 Ma. As shown below, this lower age limit underestimates the actual age of the dikes.

U–Pb ages of zircons from hornblende-dioritic enclaves in a composite dike (MR091)

Two samples of dikes representative of the CMB dike swarm were chosen for U–Pb geochronology. The sample locations are given in Fig. 2. The chemical composition of both samples is given in Table A2 . The first sample (MR 091) is an enclave-bearing composite dike that contains hornblende-dioritic enclaves within a tonalitic matrix. The second sample (MR 085), a concordant syntectonic muscovite-bearing granite dike, was chosen to determine the age of the granitic end-member of the investigated dike swarm. The enclaves of the composite dike contain abundant dark purple magmatic zircon crystals with a short prismatic morphology and strongly developed prismatic faces (G1 type of PUPIN, 1980) (Fig. 5). Superficial zircon resorption and microcracking are widespread. None of the crystals appears to contain inherited cores, but optical detection was disturbed by the strong color of most of the zircon grains. U–Pb analyses revealed very high U and

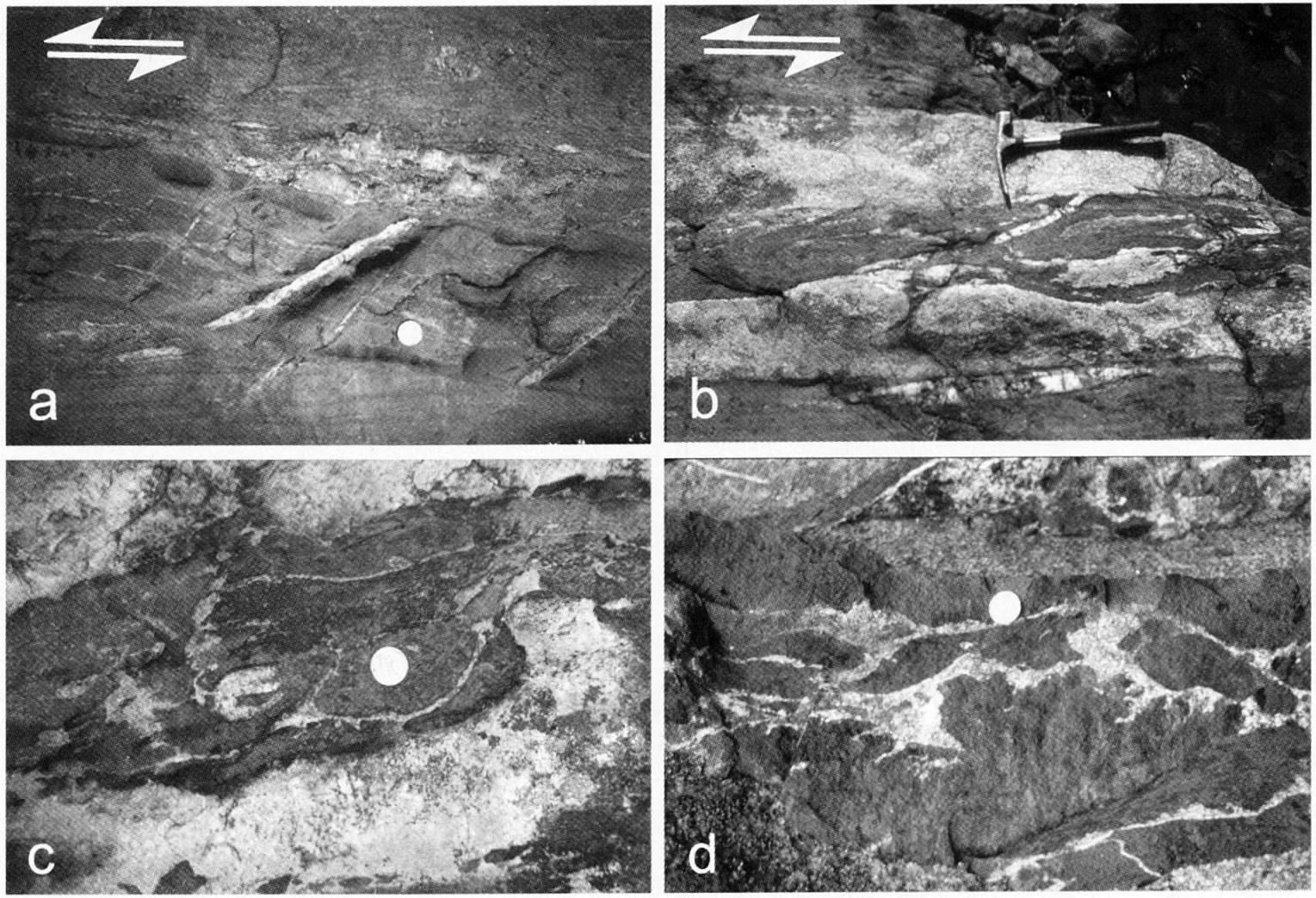

Fig. 3 Internal structure of synkinematic CMB dikes. (a) en-echélon tension gashes filled with former granitic to tonalitic melts derived from the mylonitized partially melted wall rock. Tension gashes indicate sinistral sense-of-shear within the subvertically dipping CMB mylonites. Note reaction rims at dike margins and at border of tension gashes. Swiss 5 Franc coin for scale. (b) Asymetrically sheared composite dike with dm-wide rim of granitic to tonalitic melts. Sinistral CMB-shearing induced opening of tension gash within mafic dike (center) that was that was filled with melts derived from partial melting of the wall rock. (c) Virtually undeformed composite dike showing magmatic mingling and folding. Swiss 5 Franc coin for scale. (d) Partly consolidated mafic melts of hornblende-dioritic composition are fragmented within a matrix of leucocratic melt to form enclaves or 'schollen'. The leucocratic melts have a granitic to tonalitic composition and are derived from partial melting of the mylonitic metasedimentary wall rock. Note that fractures in the mafic rock are filled with former partial melts (lower right) but lobate contacts at the interface indicate magma assimilation to form hybrids. Italian 100 Lira coin for scale. Location: Streambed near Cortaccio, Swiss Coord. 695800/107600). Sense-of-shear is indicated by white arrows.

Table 1 U-Pb zircon and titanite results for mafic and granitic veins. Number of analysed grains is given in brackets. Measured ratios are corrected for mass fractionation, blank and spike composition. Calculated ratios were also corrected for initial common lead using the model of STACEY and KRAMERS (1975). Pb_r – radiogenic lead, Pb_{ini} – initial lead, m – multigrain, lpr. – long prismatic, spr. – short prismatic, pr. – prisms, pyr. – pyramidal fragments, op. – opaque, euh. – euhedral grains.

	Sample	weight µg	U ppm	Pb_r ppm	Pb_{ini} ppm	Measured ratio $^{206}Pb/^{204}Pb$	Measured ratio $^{207}Pb/^{206}Pb$	Measured ratio $^{208}Pb/^{206}Pb$	Calculated ratio $^{207}Pb/^{235}U$	Calculated ratio $^{206}Pb/^{238}U$	Calculated ratio $^{207}Pb/^{206}Pb$	Apparent Age (Ma) Corr. coeff.	Apparent Age (Ma) $^{206}Pb/^{238}U$	Apparent Age (Ma) $^{207}Pb/^{235}U$	Apparent Age (Ma) $^{207}Pb/^{206}Pb$
Zircon MR 091															
1	spr. pink [14]	298	4318	267	1.1	8508	0.05277	0.9604	0.2508±20	0.03563±28	0.05105±57	0.99	226	227	243
2	spr. pink [11]	187	2889	169	1.1	5348	0.05386	0.8596	0.2508±11	0.03559±16	0.05111±30	0.99	225	227	246
3	pr. frg. pink [1]	24	1344	67	1.6	1506	0.06179	0.5184	0.2682±13	0.03735±16	0.05207±26	0.87	236	241	288
4	spr. pink [1]	32	3711	221	3.4	2326	0.05800	0.7817	0.2702±15	0.03791±20	0.05169±30	0.95	240	243	272
5	pr. op. [2]	34	2843	147	3.9	1601	0.06128	0.5457	0.2722±19	0.03787±18	0.05214±37	0.69	240	245	291
6	spr. pink [1]	24	3886	237	0.7	7944	0.05316	0.8301	0.2657±11	0.03755±16	0.05132±25	0.98	238	239	255
7	spr. pink [1]	11	6849	386	8.7	1659	0.06059	0.7130	0.2666±11	0.03735±15	0.05176±24	0.94	236	240	274
8	iso. pink [1]	23	3347	200	3.1	3509	0.05544	1.1143	0.2602±15	0.03686±21	0.05170±31	0.95	233	235	252
9	spr. pink [1]	15	2161	132	2.3	1681	0.06049	0.8046	0.2739±14	0.03837±18	0.05178±27	0.91	243	246	275
10	spr. pink [1]	12	2074	114	2.3	1680	0.06048	0.5993	0.2780±15	0.03893±18	0.05178±28	0.89	246	249	275
11	pyr. pink [1]	20	1712	116	2.4	1293	0.06334	1.1337	0.2588±14	0.03606±17	0.05204±30	0.84	228	234	287
12	spr. pink [1]	35	1941	106	0.7	4108	0.05483	0.7529	0.2495±11	0.03531±15	0.05125±24	0.96	224	226	252
13	spr. pink [1]	17	3134	168	2.0	2610	0.05706	0.6787	0.2557±14	0.03604±18	0.05145±26	0.93	228	231	261
14	spr. pink [1]	64	3857	210	0.2	21383	0.05178	0.7849	0.2418±19	0.03432±27	0.05109±28	0.99	218	220	245
Zircon MR 085															
15	lpr. white [m]	24	570	22	0.1	17544	0.05261	0.1094	0.2714±16	0.03803±13	0.05177±24	0.60	241	244	275
16	pr. white [5]	38	1478	56	1.3	2286	0.05823	0.0647	0.2843±14	0.03975±15	0.05188±27	0.70	251	254	280
17	lpr. white [20]	36	289	11	0.8	958	0.06825	0.1179	0.2831±22	0.03877±16	0.05296±34	0.57	245	253	327
18	lpr white [m]	21	608	23	0.6	2559	0.05891	0.1338	0.2771±20	0.03778±16	0.05319±30	0.62	239	248	337
19	spr. white [m]	38	343	26	0.3	5997	0.08020	0.1150	0.8018±50	0.07471±35	0.07783±32	0.76	464	598	1143
20	pr. pink [17]	31	378	40	0.6	4969	0.09983	0.0637	1.4426±118	0.10781±85	0.09704±21	0.96	660	907	1568
Titanite MR 091															
21	euh. clear [m]	2034	63	6.55	2.19	85	0.2339	1.9906	0.3465±59	0.03994±20	0.06292±111	0.41	252	302	705
22	euh. clear [m]	8245	90	5.19	1.69	107	0.1873	1.5284	0.1863±54	0.02715±54	0.04976±174	0.70	173	173	183
23	euh. cloudy [m]	2853	144	11.95	8.59	64	0.2882	1.3871	0.3873±100	0.04423±37	0.06350±171	0.42	279	332	724
24	euh. cloudy [m]	2611	91	7.75	4.29	68	0.2746	1.6368	0.3411±78	0.03885±24	0.06367±150	0.40	246	298	730

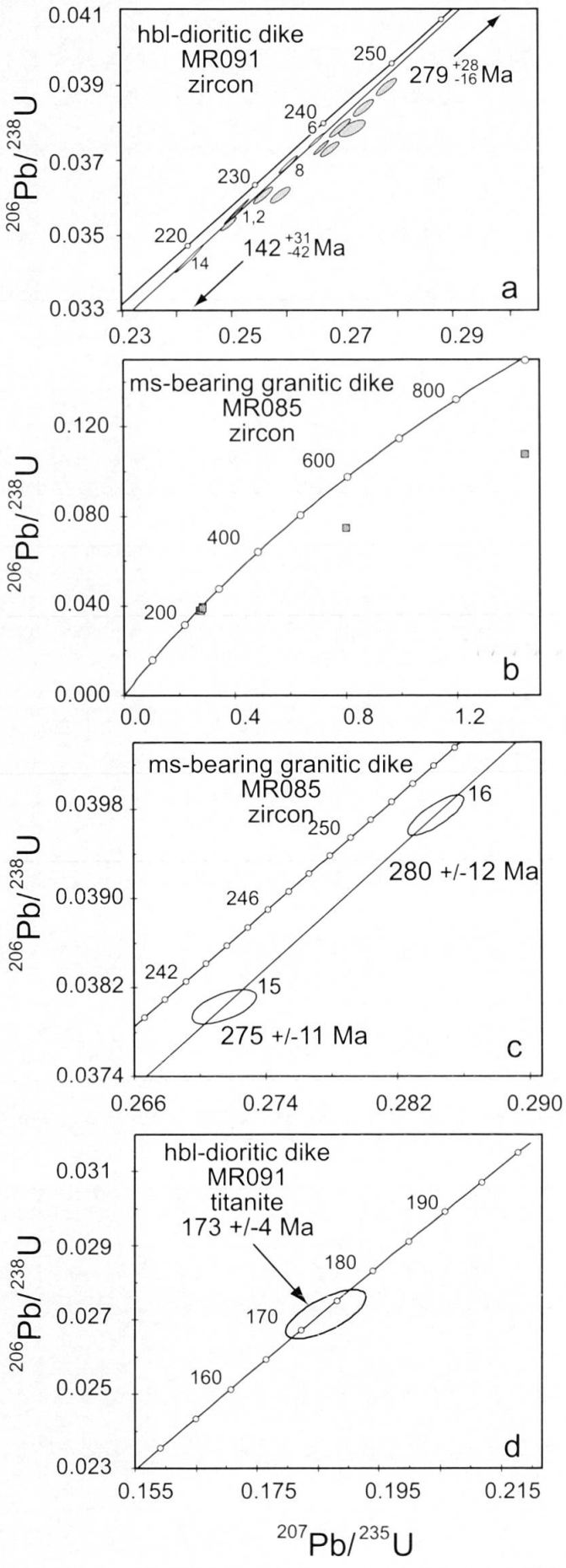

Th contents ($^{208}Pb/^{206}Pb \leq 1$). Very high U concentrations (up to 6800 ppm) in some of the zircons are probably due to (U,Th)-rich inclusions not removed during air abrasion (Fig. 5a).

Inclusion-bearing zircons are not the best candidates for a U–Pb study, but given the high retentivity of zircon under upper amphibolite-facies conditions, single zircon dating provided the best method for dating the intrusion of the dike. Because of their proximity to concordia, five high-precision analyses (1, 2, 6, 8, 14 in Table 1) of single grains, pyramidal ends or multigrain fractions of euhedral grains were chosen that yielded a discordant, but relatively coherent data pattern (Fig. 4a). The analyses plot close to the concordia line, indicating differential non-zero age Pb-loss and $^{207}Pb/^{206}Pb$ ages that cluster about 245–255 Ma. Due to their proximity to the concordia line, the influence of zircon inheritance on the individual analyses is assumed to be negligible. The discordant U–Pb data therefore provides information about the maximum age of zircon crystallization. The upper intercept of the calculated discordia line at 279 +28/–16 Ma (2σ, using GEODATE by EGLINGTON and HARMER, 1991) is a first constraint on the age of the syntectonic dikes. The lower intercept in Fig. 4a projects towards 142 +32/–42 Ma on the concordia line and overlaps within error with a concordant titanite age (analysis 22) from the same sample (Fig. 4d).

U–Pb ages of zircons from a granitic dike (MR085)

The zircon population of the muscovite-bearing granite dike (sample MR085) includes a variety of morphological types ranging from long- to short-prismatic clear crystals and including grains that display apparent cores and overgrowths (Fig. 6). The isotopic signature of these magmatic zircons is different from those of the hornblende-dioritic enclave of the composite dike (sample MR 091), as U-contents and $^{208}Pb/^{206}Pb$ ratios are significantly lower (Table 1). Typically, the zircons show at least one inherited component of Proterozoic

← *Fig. 4* (a) U–Pb concordia diagrams of zircons from hornblende dioritic enclaves in syntectonic composite (MR091) and (b, c) granitic (MR085) dikes at the CMB Line. Note that analyses 15 and 16 in (c) fall onto the discordia line calculated in (a) for zircons from the composite dike (MR091) (calculated using analyses 1,2,6,8, and 14) which is plotted for comparison only. (d) U–Pb concordia diagram for metamorphic titanite from syntectonic Early Permian composite dike (MR091). Ellipses indicate 2σ error.

age (19, 20) (Fig. 4b). Analyses 15 and 16 of long-prismatic, euhedral grains are not affected by zircon inheritance but are significantly discordant (Fig. 4c). These two discordant multi-grain fractions yield $^{207}Pb/^{206}Pb$ ages of 275 ± 11 Ma (15) and 280 ± 12 Ma (16), respectively (Fig. 4c). Most interestingly, they plot exactly on the 279 +28/–16 Ma discordia line that constrains the age of the composite dike. Taking the $^{207}Pb/^{206}Pb$ age of analyses 15 and 16 as a constraint for the age of dike emplacement, the most likely interpretation is that the granitic dike intruded at about 275–285 Ma. The striking similarity of these ages with the zircon ages of the hornblende dioritic enclave of the composite dike suggests that both the composite and granitic dike share a common intrusive and metamorphic history.

U–Pb ages of titanite from hornblende-dioritic enclaves in a composite dike (MR091)

The hornblende-dioritic enclave of the composite dike (MR091) contains abundant light-yellow to honey-yellow, idioblastic, lozenge-shaped titanite. Back-scattered electron imaging of these grains revealed no detectable internal zonation or polyphase overgrowths. We analysed four multi-grain titanite fractions. The grains comprising each fraction were hand-selected to be of identical shape and clarity. One fraction of light-yellow, clear titanites yields a concordant age of 173 ± 4 Ma (Fig. 4d), whereas three additional fractions of more cloudy varieties project towards an upper intercept at about 1.3 Ga. This paper focuses on the interpretation of the concordant data point (22) only, because the three other analyses (21, 23, 24) were strongly affected by minute zircon and apatite inclusions detected by electron microprobe imaging. The difference in age of about 100 Ma obtained for the 279 +28/–16 Ma zircon and the 173 ± 4 Ma titanite of the same sample shows that these minerals either grew at different times or that the titanite age represents a post-intrusive cooling age. Microstructural observations revealed a prominent retrogressive overprint of the primary, magmatic amp + pl + qtz + ep + hem-ilm + ap + zrn ± bt assemblage of the mafic dikes. Magmatic hornblende is partly replaced by secondary biotite, indicative of a lower amphibolite/upper greenschist facies overprint. Coeval breakdown of ilmenite exsolutions within the tschermakitic to ferro-magnesian hornblendes (LEAKE, 1978) is the inferred source of Ti for the neocrystallization of titanite. Therefore, the concordant titanite age of 173 ± 4 Ma is consistent with subsolidus titanite growth during the Jurassic.

EMP and CL imaging

To constrain the mechanisms that led to strong partial Pb-loss within the analyzed zircons, we used back-scattered electron (BSE) and cathodoluminescence (CL) imaging to investigate grains from the same splits used for U–Pb dating. CL imaging revealed irregular feather-like, convolute zoning and partial recrystallization within euhedral zircons of the hornblende-dioritic dikes (MR091). Oscillatory zoning or zircon growth around pre-existing cores is completely absent (Fig. 5).

Convolute zoning is uncommon in igneous and metamorphic zircon, and its influence on U–Pb data is not completely understood (PIDGEON et al., 1998). The hornblende-dioritic dikes at the CMB intruded a sillimanite grade metasediment at fairly high melt temperatures. Interaction of the mantle-derived mafic melt with partially melted wall rock is inferred to have caused rapid changes in melt and fluid composition. It is therefore conceivable that the formation of highly contorted convolute zoning in zircon reflects closed-system zircon recrystallization and fluid redistribution during early, high-temperature zircon crystallization (PIDGEON et al., 1998). Hence, we interpret the U–Pb ages of the strongly abraded zircons to record the timing of zircon crystallization from the melt and hence the timing of crystallization of the composite dikes. This process of closed-system recrystallization has to be distinguished from (fluid-assisted?) secondary rim-to-core open-system recrystallization that results in a stable, U-poor zircon. Zones of transgressive open-system recrystallization associated with trace element-loss are documented in Fig. 5 as homogeneous marginal bands at the upper rim of the zircon grain. These zones discordantly truncate central parts of convolute banding and replace primary zircon by featureless, recrystallized zircon. We infer that subsequent to rapid Pb-loss from highly metamict zones, the crystal structure was locally annealed by late-stage rim-to-core recrystallization and precipitation processes. The BSE image in Fig. 5a shows an ingression of a porous zircon structure ('sponge-structure') parallel to former growth zones with numerous inclusions of a (U/Th)-silicate. This secondary transformation is distinct from the one described above because high-U concentrations are retained within the zircon lattice. Consequently, (sub-)magmatic convolute zonation and precipitation of trace elements were most likely governed by closed-system behaviour of zircon as evident from high (U, Th)-concentrations preserved within individual zircon grains. Over time, zones of high trace ele-

ment concentration became metamict and provided pathways for rapid radiogenic Pb-loss.

CL patterns of zircons from the granitic dikes (MR 085) are completely different and demonstrate the complexity of multiple zircon generations within a crustally derived granitic melt. Three types of internal structures could be distinguished: Long prismatic, euhedral grains in Fig. 6a show magmatic growth zonation and lack inherited cores or overgrowths. Fractions of these grains (analyses 15 and 16) provide constraints on the emplacement age of the granite dikes. Prismatic grains (analyses 19, 20) reveal different generations of inherited cores surrounded by an irregularly zoned domain (Fig. 6b). A third type of internal structure is displayed in Fig. 6c in which an inner domain of magmatic fine-scaled oscillatory zoning is truncated by a domain of sector zoning followed by a narrow rim with no CL. The mechanisms of Pb-loss within the zircons of the granitic dike are difficult to ascertain. The absence of primary convolute zoning in zircons from the granit-

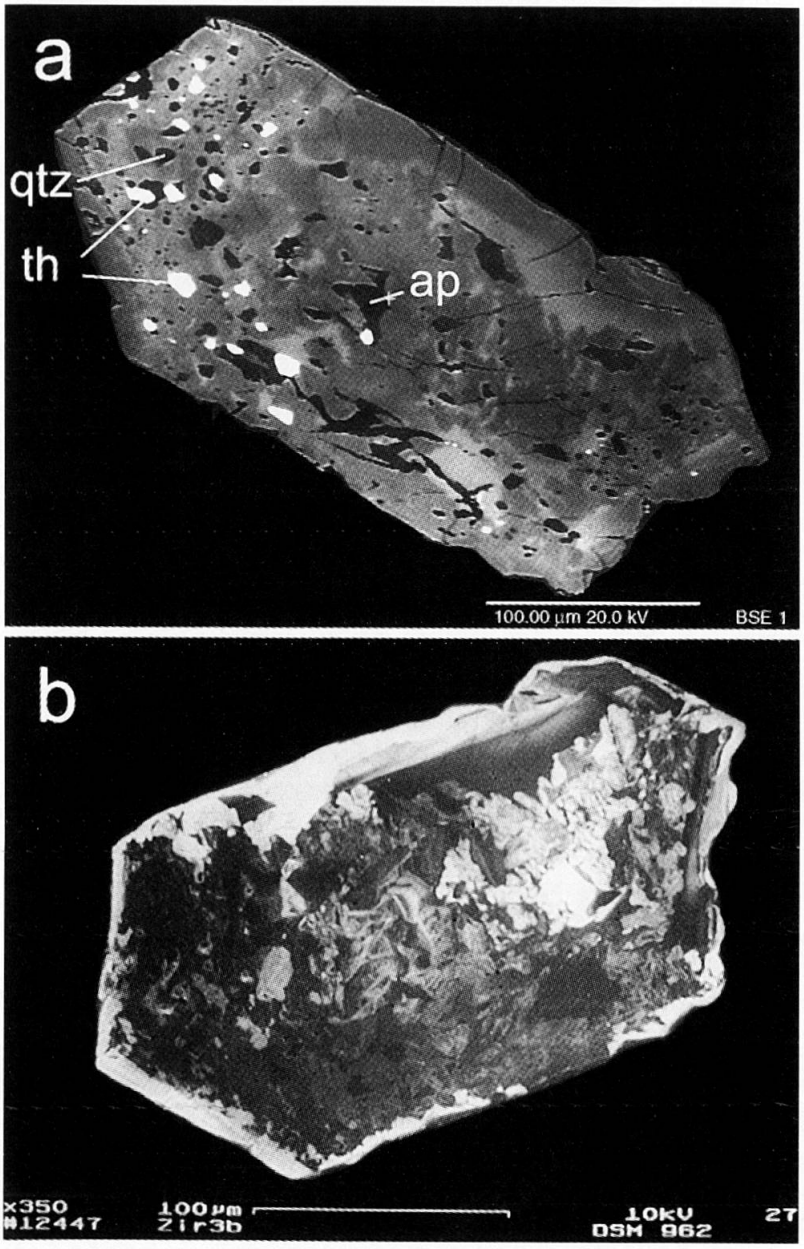

Fig. 5 (a) Back-scatter electron image of zircon from hornblende-dioritic enclaves in the composite dike before air abrasion. Note three different domains: i) porous outer zone (upper left) following euhedral crystal faces with inclusions of a U–Th silicate (th), quartz (qtz) and apatite (ap), ii) secondary rim-to-core recrystallization of low-U zircon marked by featureless dark grey zone (upper right) iii) (sub-)magmatic convolute zoning in internal part of the zircon inferred to have retained primary age information (right center). (b) Cathodoluminescene image of the same grain as shown in (a) with contorted REE-enriched bands (convolute zoning). Metamictization along high-U bands is inferred to provide rapid pathways for Pb-loss.

ic dike that has been documented for MR091 allows some inferences concerning the T-X-conditions at the time of dike emplacement. As both dikes investigated in this study intruded the same lower crustal environment and experienced the same series of metamorphic events within the CMB mylonites, primary differences in composition and melt temperatures (associated with different fluid mobilization in the country rock) probably played an important role during the formation of zoning patterns in magmatic zircon.

To conclude this section, we have shown that granitic and composite dikes along the CMB Line intruded contemporaneously in Early Permian time (275–285 Ma). This suggests that there is a link between these dikes and the Early Permian gabbro-diorites at the rim of the Mafic Complex in originally deeper parts of the IVZ exposed to the southwest (Fig. 1). In the next section, we use geochemical data to explore this possible link and the mechanisms by which melts evolved within the lower and intermediate southern Alpine crust.

Chemistry of CMB dikes and stocks

The members of the CMB dike swarm fall into three petrographically distinct populations: (1) hornblende-dioritic dikes and stocks, (2) granitic dikes and (3) composite dikes showing magmatic mingling of the two aforementioned end-members. Geochemically, the dike swarm represents a medium to high-K calc-alkaline suite that spans the whole range from monzo-gabbros via diorites and granodiorites to granites (Fig. 7 and BORIANI et al., 1974; GIOBBI ORIGONI et al., 1988; PINARELLI et al., 1988; BORIANI et al., 1995). This wide range of chemical composition suggests that the CMB dike swarm is the genetic link between dominantly mantle-derived rocks from the rim of the Mafic Complex of the IVZ and hybrid (crust- and mantle-derived) granitoids of the SCZ.

MAJOR ELEMENT COMPOSITION AND CLASSIFICATION OF THE SAMPLES

The major element compositions of the analyzed samples (Table A1) fall within the field of the CMB dike swarm when plotted on the TAS diagram and the AFM triangular plot where they display a large compositional gap as expected for end members of the intrusive suite (Fig. 7). Because of strongly contrasting differentiation indices (e.g. Si and Zr contents, rare earth element (REE) fractionation, Eu-anomaly, and ratios of Rb/Sr and Nb/Y, Table A1) mafic stocks are interpreted to represent the least evolved and mafic enclaves the most chemically evolved samples of hornblende-diorites. The leucocratic matrix in the composite dikes, though poor in modal K-feldspar, is chemically almost identical to the composition of the muscovite-bearing granitic dikes.

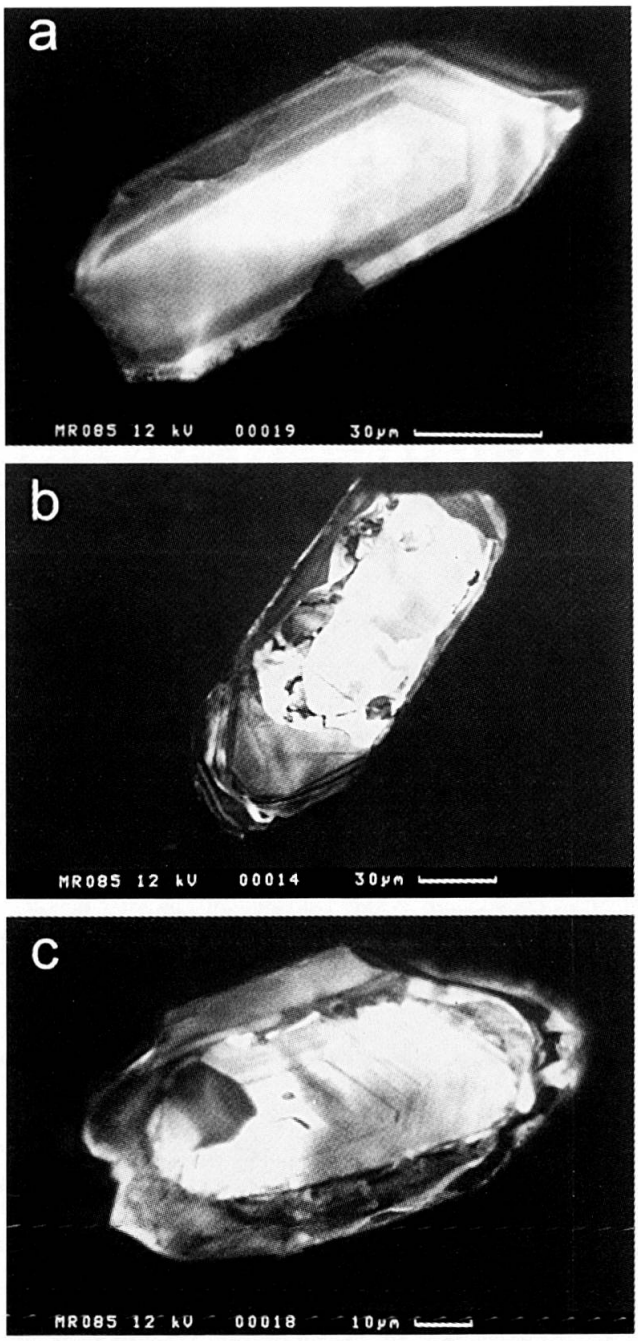

Fig. 6 Cathodoluminescence (CL) images of zircons from muscovite-bearing granite dike (MR085). (a) euhedral prismatic zircon used for analyses 15 and 16. These zircons preserve a magmatic zonation and lack any kind of inherited cores or overgrowths. (b) Euhedral zircon containing rounded inherited cores (center). Cores sit within an irregularly zoned internal domain that itself is rimmed by a low-CL domain at the pyramidal ends of the grain. (c) Magmatic oscillatory zoning in the center is truncated by dark gray bands of less regularly zoned zircon and a narrow rim showing no CL.

TRACE ELEMENT DISTRIBUTION

Trace element compositions of the granitic samples are close to mean values of S-type granite (WHALEN et al. 1987) and amphibolite facies crust (WEAVER and TARNEY, 1981). A comparison between the incompatible element signatures of the granitic samples with the metasediments of the IVZ (data from SCHNETGER et al., 1994) clearly demonstrates their intimate relationship (Fig. 8a). However, two significant differences in their incompatible element signatures exist: (1) the relatively high Sr contents of the partial melts and (2) their relatively low contents of Ti, Y and heavy REE (HREE, Er-Lu in this plot represented by Yb). These differences are related to the metamorphic conditions during segregation:

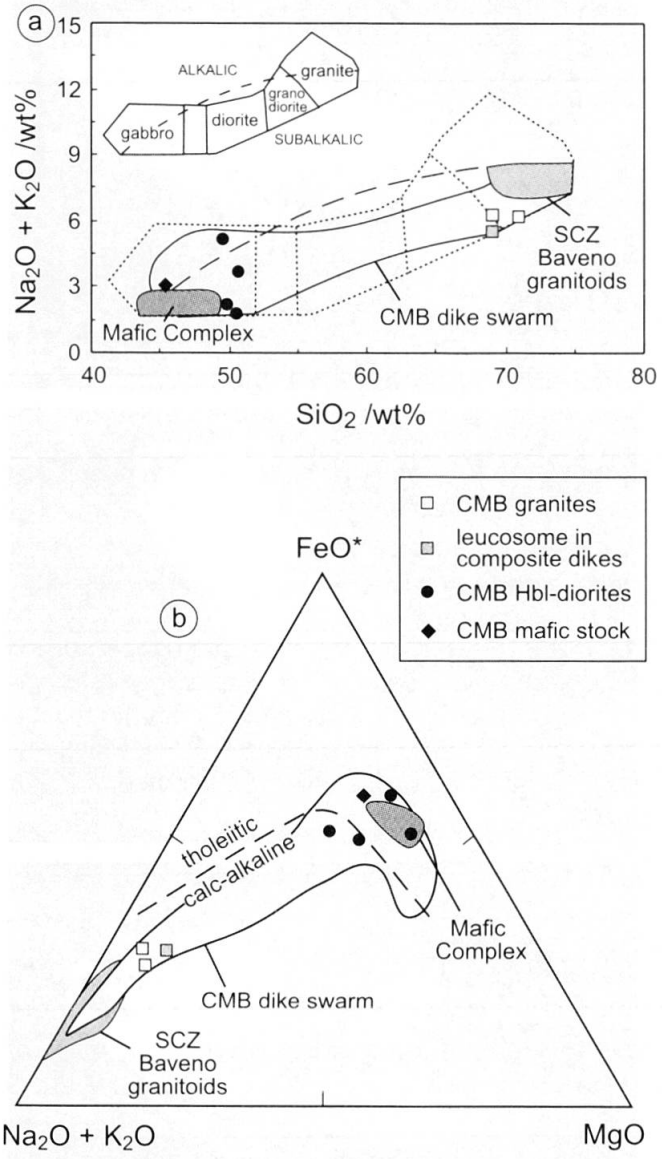

Fig. 7 (a) Total alkali vs. SiO_2 (TAS) plot with classification of subalkalic plutonic rocks after WILSON (1989). Note that pyroxene-free CMB hornblende-dioritic dikes plot in the gabbro field due to high modal amounts of primary hornblende and biotite that are low in SiO_2 with respect to pyroxene. These low-SiO_2 hornblende-dioritic dikes (filled circles and diamond) are therefore interpreted as being close to one end-member composition of the CMB dike swarm. (b) AFM ternary plot with tholeiitic to calc-alkaline division. Data defining fields of Mafic Complex, CMB dike swarm and Baveno granitoids in (a) and (b) are from BORIANI et al. (1974), GIOBBI ORIGONI et al. (1988), PINARELLI et al. (1988), BORIANI et al. (1992), BORIANI et al. (1995), SINIGOI et al. (1994) and ZURBRIGGEN (1996).

(1) Sr-enriched partial melts necessitate a high degree of melting of feldspar and suggest melting in the presence of a fluid phase (HARRIS and INGER, 1992). This is in accord with the aforementioned reaction:

muscovite + quartz + plagioclase + water = sillimanite + melt

as proposed for the mylonitic host rock. Large melt fractions (up to 45 vol%) are expected for vapour-present melting by CLEMENS (1984) and HARRIS and INGER (1992) and are accounted for by the widespread occurrence of granites, pegmatites and pegmatoids that are spatially associated with the CMB Line (Fig. 2 and e.g. ZURBRIGGEN, 1996).

(2) Y and HREE depletion of partial melts with respect to their protolith manifests the presence of garnet as a stable restite phase, whereas lower Ti contents of the partial melt suggest that biotite was also a restitic phase during melt segregation. Both phases are ubiquitous in the mylonitic host rock.

Figure 8b displays the chondrite-normalized REE pattern of the hornblende-dioritic and muscovite granite end-members of the CMB dike swarm. The REE patterns of the granite dikes are subparallel and show a strong fractionation from light REE (LREE: La–Nd) to HREE ($(La/Yb)_N$ = 23–40) and no significant Eu-anomaly ($(Eu/Eu^*)_N$ = 0.85–1.2) when normalized to chondrite (N). These features support the hypothesis that granitic melts were segregated from a garnet-bearing protolith and indicate that their composition was not affected by differentiation involving feldspar fractionation, i.e., granitic melts were true partial melts from the metasedimentary host rock.

The REE patterns of hornblende-diorites (Fig. 8b) show a systematic REE variation, with the LREE becoming successively enriched from the mafic stock sample to the mafic enclave sample, concurrent with successive depletion of HREE. This systematic variation from slightly fractionated REE patterns displayed by the mafic stock ($(La/Yb)_N$ = 3.8) to moderately fractionated REE patterns of the mafic enclave ($(La/Yb)_N$ = 9.0) is

taken as evidence that mixing of the hornblende-diorite with the highly REE-fractionated CMB granites occurred during their chemical evolution. Fractional crystallization of hornblende is a process that accounts for the tilt between steep LREE patterns and flat MREE+HREE patterns of the hornblende-diorites. The lack of a significant Eu-anomaly ($(Eu/Eu^*)_N = 0.95–1.0$) suggests that plagioclase fractionation was not an important mechanism.

RELATIONSHIPS TO REGIONAL EARLY PERMIAN MAGMATISM AND SIGNIFICANCE OF THE CMB DIKES

Figures 8c and d display the incompatible element signatures of CMB dikes in comparison with those from the SCZ Baveno granitoids and mafic rock samples of the IVZ Mafic Complex. Rocks of comparable composition and petrography as the hornblende-diorites of the CMB dike swarm occur as enclaves and dikes of similar age within the Early Permian dioritic rim of the Mafic Complex (SINIGOI et al., 1994). As shown in Fig. 8d, the mafic stock sample (representing the most primitive composition of the CMB dike swarm) has an almost identical incompatible element signature as the Early Permian enclaves and dikes of the Mafic Complex. This suggests a common origin during the late stages of Early Permian magmatic underplating. Only the positive Rb-anomaly is unique for the CMB dike swarm and may be attributed to the absorption of metamorphic fluids during magma ascent through deep-crustal levels where biotite dehydration breakdown reactions at the amphibolite-granulite facies transition may have produced Rb-rich fluids.

The SCZ granitoids consist of several granodioritic and granitic plutons that were emplaced during Early Permian time within intermediate to upper crustal levels. A common genesis by fractional crystallization processes has been proposed for this suite (BORIANI et al., 1992). Isotope data indicate that these rocks were hybrid magmas comprising both mantle and crustal components (PINARELLI et al., 1988). The granitoids are believed either to have developed by fractional crystallization of mantle-derived melts from the same source that formed the Mafic Complex (PIN and SILLS, 1986; VOSHAGE et al., 1990; BORIANI et al., 1992; BORIANI et al., 1995) or to result from dehydration melting of a fertile crust, where partial melts mixed with mafic melts (SINIGOI 1994). Figure 8c shows the incompatible element signature of the CMB hornblende-diorites compared to representative samples of the SCZ Baveno granitoids (see compilation in BORIANI et al., 1992). The generally lower LILE contents of the CMB hornblende-diorites as well as their lack of pronounced negative Sr- and Ti-anomalies are characteristic of the SCZ granitoids and constrain the possible differentiation processes. Assimilation of LILE-rich and Ti-poor partial melts represented by the CMB granitoids, and fractional crystallization of plagioclase and hornblende are shown below to be viable processes to produce the SCZ granitoid pattern from the pattern observed in the CMB hornblende-diorites.

Trace element modelling

To test these petrogenetic hypotheses, we calculated the effects of the individual mechanisms (partial melting, assimilation of partial melts, fractional crystallization) on the Rb, Sr, Nb and Y concentrations of the different magmas (for the constituting formulas and parameters see Appendix). We emphasize that applying a single set of model parameters, for example, assuming constant distribution coefficients as well as perfect AFC and FC, may grossly oversimplify the complex melting and mixing processes that might be expected for melt generation in a compositionally heterogeneous crust. However, the results obtained should be regarded as one possible mechanism that, when properly supported by independent structural and geochronological evidence, can provide additional information on melt ascent and the interaction of melts from different sources.

Figure 8e displays the starting compositions (boxes), the SCZ granitoid field and the evolution trajectories on a Nb/Y vs. Rb/Sr diagram. This plot discriminates the proposed mechanisms, as the Nb/Y ratio is an index for garnet-present partial melting as well as hornblende fractionation, whereas the Rb/Sr ratio is a common index for feldspar fractionation.

The chemical model for partial melting describes the segregation of eutectic partial melts from the IVZ metasedimentary country rock (source S in Fig. 8e) due to water-present breakdown of muscovite assuming garnet as a restitic phase and non-modal batch melting (SHAW, 1970). Extraction of a melt fraction $F_m = 30$ wt% fits the observed high-Sr, low-Y composition of the CMB granites (A in Fig. 8e). The chemical model that reproduces the SCZ granites from the CMB hornblende-diorites (X_0 in Fig. 8e) involves two evolutionary stages. During a first stage of assimilation and fractional crystallization (AFC, DEPAOLO 1981), 30% fractional crystallization of equal amounts of hornblende and plagioclase accompa-

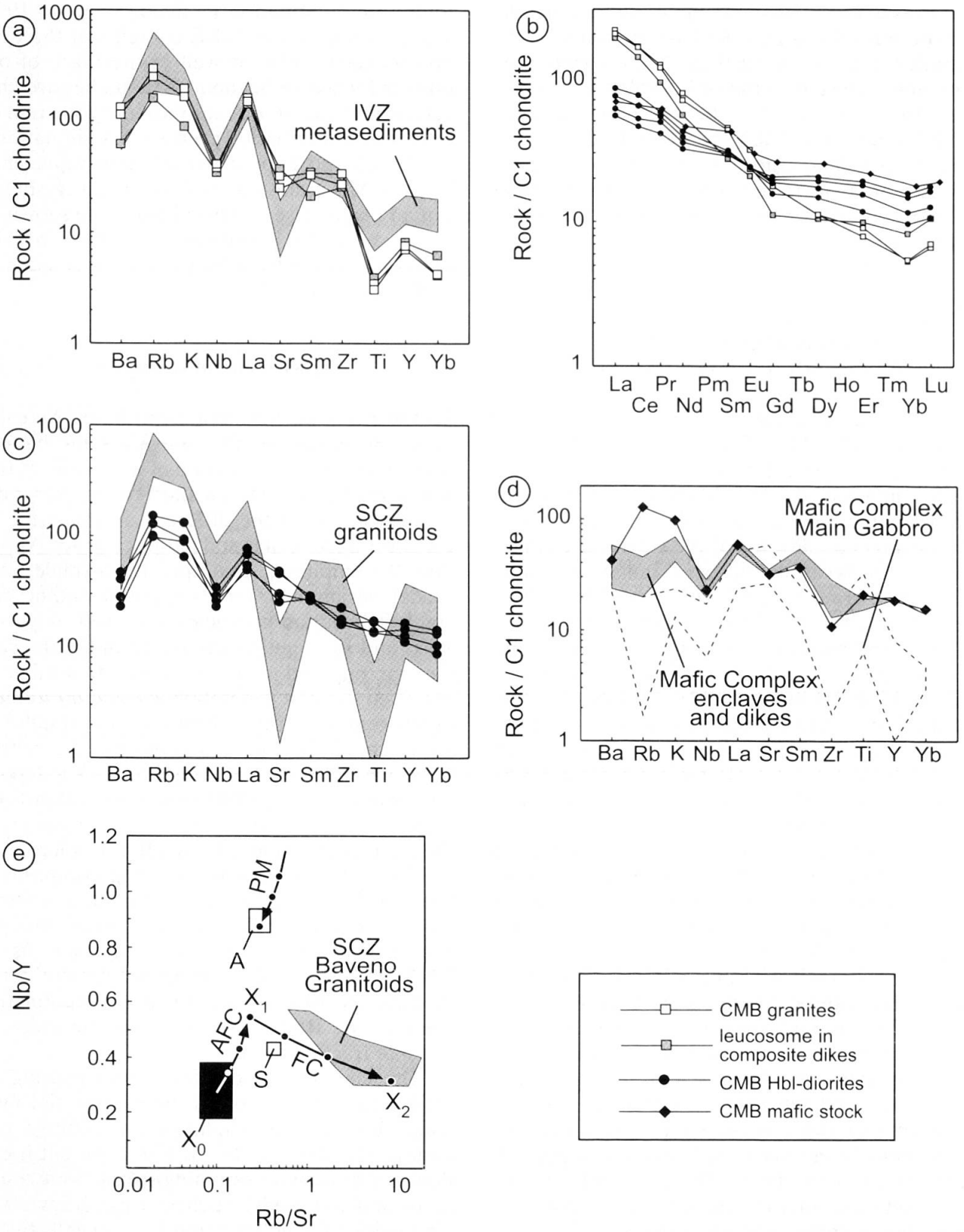

Fig. 8 (a, c, d) Chondrite-normalized incompatible element distribution (normalizing values from THOMPSON et al., 1982, and SUN, 1980) of the CMB dike swarm (for symbols see legend) and related rocks of the IVZ and CMB. (b) REE-pattern (normalizing values from EVENSEN et al., 1978) of the CMB dike swarm. (e) Nb/Y vs. Rb/Sr plot with the results of modelling the trace element composition of the CMB hornblende-dioritic and granitic dikes (see text for details). Note that the modeling results only represent one of the possible mechanisms. AFC – assimilation and fractional crystallization, PM – partial melting, FC – fractional crystallization, S – source rocks for partial melting, A – field of CMB granite dikes, X_0 – mean value of CMB hornblende diorite dikes, X_1 and X_2 are the compositions after the AFC stage (using an AFC : FC ratio r = 0.5) and the subsequent FC (r = 0) stage, respectively.

nied by 15% assimilation (assimilation-to-crystallization ratio r = 0.5) of an partial melt with the composition of the CMB-granites (assimilant A in Fig. 8e) yield an intermediate, hybrid melt (X_1 in Fig. 8e) which is significantly depleted in Y and slightly depleted in Sr. A second stage (FC) is controlled by fractional crystallization of plagioclase and minor amounts of titanite but no further crustal contamination (r = 0). After 60% fractionation, a hybrid granitic magma is obtained from the X_1 composition that is characterized by moderate Y concentrations and very low Sr contents similar to the most differentiated rocks of the SCZ Baveno granitoids (X_2 in Fig. 8e).

Discussion

Before discussing the age data, we point out that the dated samples MR091 and MR085 were collected because they contain key structural relationships within both the composite and granitic members of the syntectonic CMB dike swarm. Hence, the 'starting material' for U–Pb geochronology was less than ideal from a mineralogical standpoint and the ages of the two U–Pb zircon data sets presented here are not as accurate as those obtained in recent high-precision U–Pb studies (e.g. SCHALTEGGER, 1993; CORFU, 1996). Nevertheless, the ages of the two data sets are internally consistent and are also in accord with the mutual overprinting relationships of the dikes and the CMB mylonites.

The 279 +28/–16 Ma upper intercept for the least discordant zircons from the hbl-dioritic enclave and the 275 ± 11 Ma and 280 ± 12 Ma $^{207}Pb/^{206}Pb$ ages for the magmatic zircon fractions from the granitic dike allow us to constrain the age of CMB diking to the Early Permian time span from 275 to 285 Ma. Thus, syn-mylonitic intrusion of the CMB dikes clearly post-dated the 321 ± 2 Ma Late Variscan intrusion of leucotonalitic dikes in the SCZ obtained from Pb–Pb step leaching of magmatic garnets (ZURBRIGGEN et al., 1998). These older dikes are related to large scale F3 folds in the SCZ that are clearly sheared by the CMB mylonites.

Following HANDY and ZINGG (1991), VAVRA and SCHALTEGGER (1999) suggested that post-granulite facies decompression and tectonic shearing caused new monazite growth in high-grade IVZ metapelites during localized partial melting that initiated at about 273 Ma. Although VAVRA and SCHALTEGGER (1999) and HENK et al. (1997) disagreed in their interpretation of the pattern of monazite ages across the IVZ, both studies indicate a Late Carboniferous regional thermal peak of metamorphism. We propose that mylonitization along the CMB Line and within associated high-temperature shear zones of the IVZ (e.g. BRODIE and RUTTER, 1987; SNOKE et al., 1999) was responsible for Early Permian oblique extension, decompression, and associated partial melting (HANDY et al., 1999). This partial melting event and related metamorphism was local, and clearly post-dated an earlier phase of leucosome generation related to the amphibolite to granulite facies regional metamorphism in the Late Carboniferous. The similar U–Pb ages obtained from the least discordant zircon analyses of the hornblende-dioritic enclave (analyses 1, 2, 6, 8, 14) and from the magmatic zircons of the muscovite-bearing granite dike (15, 16) support the idea that both are consanguineous and share a common syn- and post-magmatic history.

The close genetic relationship of the CMB dikes implied by the geochemical and isotopic age data has two major implications for the evolution of the southern Alpine continental crust: First, oblique extension of the lower southern Alpine crust took place during Early Permian time (275–285 Ma), distinctly prior to Early Mesozoic rifting. In contrast to the vigorous magmatism at all crustal levels that accompanied Early Permian transtension, magmatism associated with Early Mesozoic rifting was negligible in the IVZ (e.g. HANDY et al., 1999 and references therein). Second, the mylonites of the CMB Line acted as a conduit for the generation, ascent and differentiation of syntectonic melts. The fact that partial melting is restricted to mylonites in the vicinity of the dikes and that the partial melts back-veined the hornblende-dioritic dikes (recall Fig. 3) indicates that melt migration within the CMB mylonites was facilitated by deformation. More specifically, the accumulation of partial melts within en-echélon tension gashes on different scales (within cm-size mafic enclaves, within entire mafic dikes) and within the necks of boudinaged hornblende-dioritic dikes indicates that granitic melts migrated down normal stress gradients from source regions in the mylonitic country rock to sites where they interacted with mantle-derived melts. Back-veining involved melt-induced fracturing of the freshly crystallized mafic melts (Fig. 3 b,d), followed in some cases by mixing and assimilation of the partial melt with partly consolidated mafic melt (Fig. 3c). The hybrid melts engendered by such mixing and assimilation may occupy the compositional gap between coeval Baveno granitoids in the upper crust and gabbroic rocks within the dioritic rim of the Mafic Complex in the IVZ, consistent with the results of trace element modelling shown in Fig. 8.

Chronological, mineralogical, and geochemical data support the hypothesis that the gabbro-dioritic rocks within the SW rim of the Mafic Complex represent the source melts for the hornblende-dioritic dikes along the CMB Line. Unfortunately, Mesozoic and Alpine tectonics appear to have excised most segments of the crust in which chemical differentiation processes might have produced the granitoid rocks in the SCZ from the hybrid CMB dikes. In particular, shallower levels of the CMB Line that form a possible link with granitoid plutons in the SCZ are not exposed. The absence of such exposures hinders detailed studies of the ascent and evolution of the hybrid melts to shallower levels of the southern Alpine crust. Assimilation of partial melts and fractional crystallization are processes of chemical differentiation which might have occurred within the dikes themselves or within CMB-linked magma chambers.

In our model, lower crustal diking in Early Permian time was restricted to the originally moderately inclined CMB Line. There, the decreased fracture strength of the mylonites parallel to their foliation facilitated the rapid upward flow of transiently overpressurized melts within episodically propagating dikes (HANDY and STREIT, 1999; HANDY et al., 2001). The dikes linked to form networks that eventually drained partial melts from the fertile amphibolite facies paragneisses of the IVZ. Field observations along the Brissago segment of the CMB Line show that individual dikes and dike networks presently make up at least 20 vol% of the 2–3 km wide belt of CMB mylonites (ZURBRIGGEN, 1996). Given the evidence of rapid crystallization and sporadic melt ascent, however, a much smaller volume percent of dikes would have transported melt at any given time during diking and mylonitization.

Figure 9 depicts the CMB Line and related melts as they may have appeared in profile during Early Permian time. The figure also incorporates the available radiometric age data on magmatic

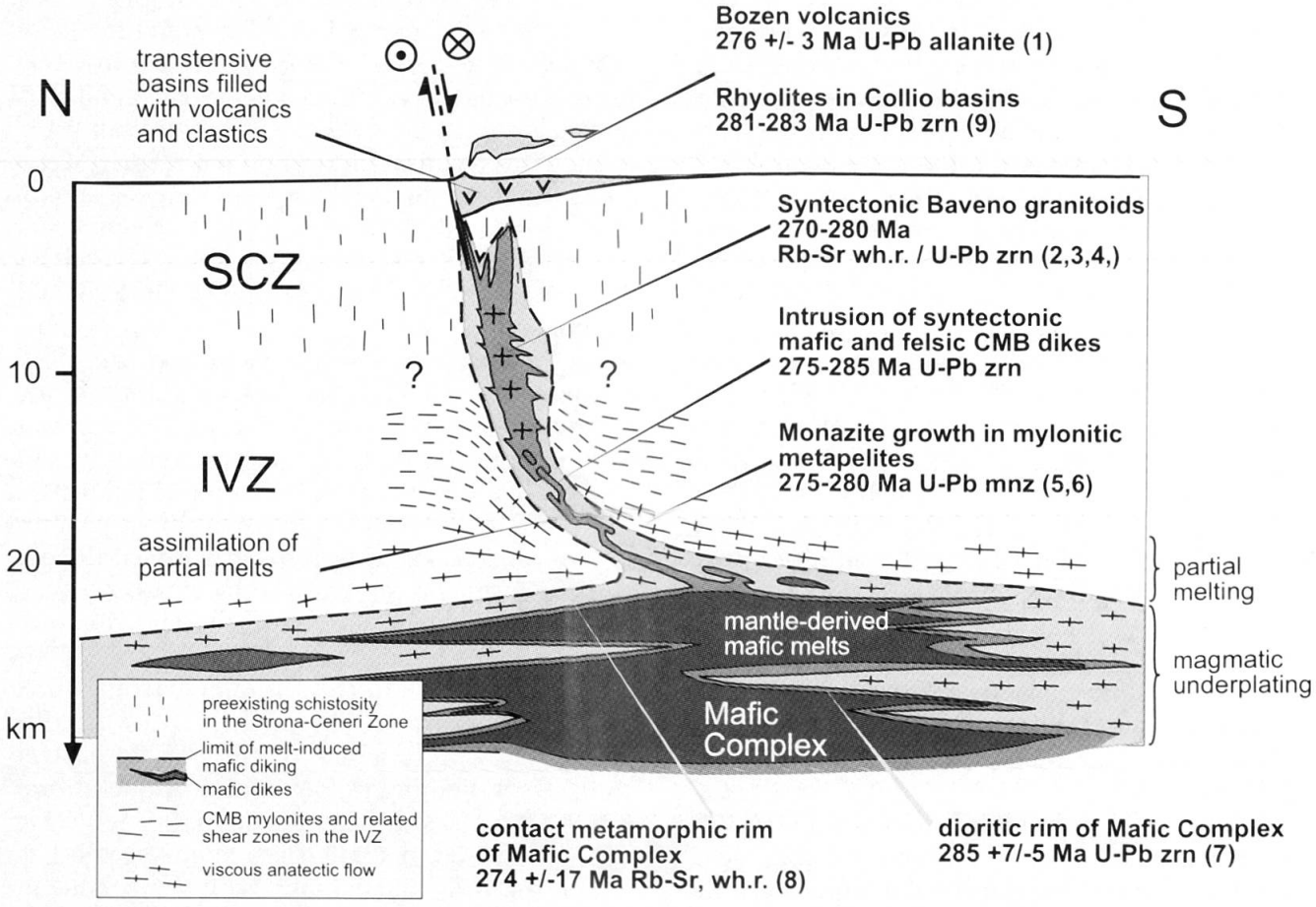

Fig. 9 Synthetic composite cross-section of the IVZ-SCZ contact as it existed in Early Permian time. The CMB Line is depicted as a moderately inclined lower crustal mylonite zone that links up with steeply dipping strike-slip faults bounding transtensive basins in the upper crust. Increasing volume proportions of partial melt with depths result in synkinematic weakening of the mylonitic crust. References for geochronological data are given by numbers in parentheses: (1) BARTH et al. (1994), (2) HUNZIKER, (1974), (3) KÖPPEL and GRÜNENFELDER (1978), (4) PINARELLI et al. (1988), (5) HENK et al. (1997), (6) VAVRA and SCHALTEGGER (1999), (7) PIN (1986), (8) BÜRGI and KLÖTZLI (1990), (9) SCHALTEGGER and BRACK (1999).

rocks in various levels of the southern Alpine crust. The section is based on a qualitative retrodeformation of the Alpine and Early Mesozoic tectonics that extensively modified the geometry of the southern Alpine basement units (HANDY et al., 1999). In this model, the CMB Line forms the locus of melt ascent within the southern Alpine continental crust.

We emphasize that the effects of Early Permian magmatism are distinct from those of Early Mesozoic rifting just prior to the opening of the Liguro-Piemontese ocean. Neocrystallization of titanite at 173 ± 4 Ma marks the time when retrograde biotite and titanite grew at the expense of primary magmatic hornblende. Titanite growth is interpreted to document the timing of when the intermediate crust was thinned and mantle rock was exhumed, primarily along the Early Jurassic Pogallo Line (HODGES and FOUNTAIN, 1984, HANDY 1987). The age of the Pogallo Line has been previously constrained to 180–210 Ma by correlating the estimated temperatures of Pogallo mylonitization with the radiometrically derived cooling curve for the southern part of the IVZ (HANDY, 1987; ZINGG et al., 1990). Since these studies, a 187.8 ± 0.5 Ma $^{40}Ar/^{39}Ar$ age for muscovite (BORIANI and VILLA, 1997) and a 170 ± 5 Ma Rb–Sr age of biotite from a hornblende-dioritic dike (PINARELLI et al., 1988) within the area of investigation have confirmed that the Early Mesozoic rifting event affected different isotopic systems. Considered in the light of past studies, our metamorphic titanite age therefore confirms that crustal thinning and basin formation in the upper crust (e.g. BERTOTTI et al., 1993) had an immediate thermal impact on the mid- to lower crustal metasedimentary rocks of the IVZ, as previously proposed by numerous workers over many years (e.g. FERRARA and INNOCENTI, 1974; HANDY, 1987).

Conclusions

Early Permian oblique extension and Early Jurassic rifting were accommodated by separate mylonite zones and are recorded by different isotopic systems in the southern Alpine basement. Early Permian deformation was accommodated by mylonitic shearing along the CMB Line. This deformation along the CMB Line was coeval with the intrusion of mantle-derived melts dated at 275–285 Ma by upper intercept U–Pb ages on zircon from syn-mylonitic composite and granite dikes. Diking at the CMB Line at 275–285 Ma post-dated regional granulite facies metamorphism during the Carboniferous and was related to the final stages of mafic underplating in the Mafic Complex of the Ivrea-Verbano Zone (HANDY et al., 1999; BARBOZA and BERGANTZ, 2000). The heat advected by the mafic dikes induced localized partial melting along the CMB Line, but probably did not cause widespread anatexis and regional metamorphism in the rest of the IVZ. Modelling one possible evolution of melt generation along the CMB mylonite zone is consistent with mixing of the mantle-derived dioritic melts with partial melts from the peraluminous mylonitic metapelites and may have produced the parental melts of the SCZ granitoids. In contrast to Early Permian CMB tectonics, Early Mesozoic rifting was accommodated by mylonitization along the Pogallo Line. These mylonites overprint the CMB-fabrics and related dikes. The Pogallo extension was responsible for the rapid decrease of metamorphic conditions in Jurassic time (HANDY, 1987), as confirmed by the 173 ± 4 Ma formation age of titanite from Early Permian hornblende-dioritic dikes.

Acknowledgements

We enjoyed fruitful discussions with Claudio Rosenberg, and Pablo Valverde-Vaquero (Univ. Giessen) on many aspects of our work. We thank Roger Zurbriggen (Bern) for his help in the initial stages of our project. Comments by U. Schaltegger (Zürich) and S. Schmid (Basel), and by two anonymous journal reviewers are gratefully acknowledged and helped to clarify certain aspects of this paper. Thanks also go to Janina Schastok for her assistance during the U–Pb analyses and to Sabine Wulf (GFZ-Potsdam) for some of the cathodoluminescence images. The financial support of the Deutsche Forschungsgemeinschaft (DFG Projects Ha 2403/1, 2403/2) is acknowledged with gratitude.

References

BARTH, S., OBERLI, F. and MEIER, M. (1994): Th–Pb versus U–Pb isotope systematics in allanite from co-genetic rhyolite and granodiorite: implications for geochronology. Earth Planet. Sci. Lett. 124, 149–159.

BARBOZA, S.A. and BERGANTZ, G.W. (2000): Metamorphism and anatexis in the Mafic Complex contact aureole. Ivrea Zone, northern Italy, J. Petrol. 41, 8, 1307–1327.

BERTOTTI, G., PICOTTI, V., BERNOULLI, D. and CASTELLARIN, A. (1993): From rifting to drifting: tectonic evolution of the South-Alpine upper crust from the Triassic to the Early Cretaceous. Sediment. Geol. 86, 53–76.

BORIANI, A. and SACCHI, R. (1973): Geology of the junction between the Ivrea-Verbano and the Strona-Ceneri Zones. Mem. Ist. Geol. Mineral. Univ. Padova 28, 1–35.

BORIANI, A., COLOMBO, A., GIOBBI ORIGONI, E. and PAGLIANI, G.P. (1974): The "Appinite Suite" of Massiccio dei Laghi (Northern Italy) and its relationship to the regional metamorphism. Rend. Soc. It. Mineral. Petrol. 30, 2, 893–917.

BORIANI, A., BIGIOGGERO, B. and ORIGONI GIOBBI , E. (1977): Metamorphism, tectonic evolution and ten-

tative stratigraphy of the 'Serie dei Laghi'. Geological Map of the Verbania area (Northern Italy). Mem. Soc. Geol. It. 32, 1–26.

BORIANI, A., BURLINI, L., CAIRONI, V., GIOBBI ORIGONI, E., SASSI, A. and SESANA, E. (1988): Geological and Petrological studies on the Hercynian Plutonism of Serie dei Laghi – geological map of its occurrence between Valsesia and Lago Maggiore (N-Italy). Rend. Soc. Ital. Mineral. Petrol. 43, 2, 367–384.

BORIANI, A., BURLINI, L. and SACCHI, R. (1990): The Cossato-Mergozzo-Brissago Line and the Pogallo Line (Southern Alps, Northern Italy) and their relationships with the late-Hercynian magmatic and metamorphic events. Tectonophysics 182, 91–102.

BORIANI, A., CAIRONI, V., GIOBBI ORIGONI, E. and VANNUCCI, R. (1992): The Permian intrusive rocks of the Serie dei Laghi (Western Southern Alps), Acta Vulcanol. 2 , 73–86.

BORIANI, A., GIOBBI ORIGONI, E. and PINARELLI, L. (1995): Paleozoic evolution of southern Alpine crust (northern Italy) as indicated by contrasting granitoid suites. Lithos 35, 47–63.

BORIANI, A.C. and VILLA, I. M. (1997): Geochronology of regional metamorphism in the Ivrea-Verbano Zone and Serie dei Laghi, Italian Alps. Schweiz. Mineral. Petrogr. Mitt. 77, 381–401

BRODIE, K.H. and RUTTER, E.H. (1987): Deep crustal extensional faulting in the Ivrea Zone of northern Italy. Tectonophysics 140, 193–212.

BÜRGI, A. and KLÖTZLI, U. (1990): New data on the evolutionary history of the Ivrea Zone (northern Italy). Bull. Swiss Assoc. Petrol. Geol. Eng. 56 (103), 49–105.

CASSINIS, G., TOUTIN-MOURIN, N. and VIRGILI, C. (1995): A general outline of the Permian continental basins in southwestern Europe. In: SCHOLLE, P.A., PERYT, T.M. and ULMER-SCHOLLE, D.S. (eds): Sedimentary Basins and Economic Resources, Springer, Berlin.

CLEMENS, J.D. (1984): Water contents of silicic to intermediate magmas. Lithos 17, 273–287.

CORFU, F. (1996): Multistage zircon and titanite growth and inheritance in an Archean gneiss complex, Winnipeg River Subprovince, Ontario. Earth Planet. Sci. Lett. 141, 175–186.

DEPAOLO, D.J. (1981): Trace element and isotopic effects of combined wallrock assimilation and fractional crystallization. Earth Planet. Sci. Lett. 53, 189–202.

EGLINGTON, B.M. and HARMER, R.E. (1991): GEODATE – a program for the processing and regression of isotope data using IBM-compatible microcomputers (Division of Earth, Marine and Atmospheric Science and Technology, Pretoria, South Africa).

EVENSEN, N.M., HAMILTON, P.J. and O'NIONS, R.K. (1978): Rare-earth element abundances in chondritic meteorites. Geochim Cosmochim. Acta 42, 1199–1212.

FERRARA, G. and INNOCENTI, F. (1974): Radiometric age evidences of a Triassic thermal event in the southern Alps. Geol. Rundsch. 63, 572–581.

GEBAUER, D. (1993): The Pre-Alpine evolution of the continental crust of the Central Alps-an overview. In: VON RAUMER, J. F. and NEUBAUER, F.(eds): Pre-Mesozoic Geology in the Alps. Springer Verlag, 93–117.

GIOBBI ORIGONI, E., BOCCHIO, R., BORIANI, A., CARMINE, M. and DE CAPITANI, L. (1988): Late-Hercynian mafic and intermediate intrusives of Serie dei Laghi (N-Italy). Rend. Soc. Ital. Mineral. Petrol. 43, 395–410.

HANDY, M.R. (1987): The structure, age and kinematics of the Pogallo Fault Zone; Southern Alps, northwestern Italy. Eclogae geol. Helv. 80, 593–632.

HANDY, M.R. and ZINGG, A. (1991): The tectonic and rheological evolution of an attenuated cross section of the continental crust: Ivrea crustal section, southern Alps, northwestern Italy and southern Switzerland. Geol. Soc. Am. Bull. 103, 236–253.

HANDY, M.R., FRANZ, L., HELLER, F., JANOTT, B. and ZURBRIGGEN, R. (1999): Multistage accretion and exhumation of the continental crust (Ivrea crustal section, Italy and Switzerland). Tectonics 18, 6, 1154–1177.

HANDY, M.R. and STREIT, J. (1999): Mechanics and mechanisms of magmatic underplating: inferences from mafic veins in deep crustal mylonites. Earth Planet. Sci. Lett. 165, 271–286.

HANDY, M.R., MULCH, A., ROSENAU, M. and ROSENBERG, C.L. (2001): The role of fault zones and melts as agents of weakening, hardening and differentiation of the continental crust: a synthesis. In: HOLDSWORTH R.E., STRACHAN, R.A., MAGLOUGHLIN, J.F. and KNIPE, R.J. (eds): The Nature and Tectonic Significance of Fault Zone Weakening. Geol. Soc. London Spec. Publ. 186, 305–332.

HARRIS, N.B.W. and INGER, S. (1992): Trace element modelling of pelite-derived granites. Contrib. Mineral. Petrol. 110, 46–56.

HENK, A., FRANZ, L., TEUFEL, S. and ONCKEN, O. (1997): Magmatic Underplating, Extension and Crustal Reequilibration: Insights from a Cross-Section through the Ivrea Zone and Strona-Ceneri Zone, Northern Italy. J. Geol. 105, 367–377.

HODGES, K.V. and FOUNTAIN, D.M. (1984): Pogallo Line, southern Alps, northern Italy: An intermediate crustal level low-angle normal fault? Geology 12, 151–155.

HUNZIKER, J.C. (1974): Rb–Sr and K–Ar age determinations and the Alpine tectonic history of the western Alps. Mem. Ist. Geol. Mineral. Univ. Padova 31, 1–55.

HUNZIKER, J.C., DESMONS, J. and HURFORD, A.J. (1992): Thirty-two years of geochronological work in the Central and Western Alps: a review on seven maps. Mémoires de Géologie (Lausanne) 13, 59 pp.

KÖPPEL, V. (1974): Isotopic U–Pb Ages of Monazites and Zircons from the Crust-Mantle Transition and Adjacent Units of the Ivrea and Ceneri Zones (southern Alps, Italy). Contrib. Mineral. Petrol. 43, 55–70.

KÖPPEL, V. and GRÜNENFELDER, M. (1978): Monazite and Zircon U–Pb Ages from the Ivrea and Ceneri Zones (southern Alps, Italy). Mem. Sci. Geol. 33, 55–70.

KROGH, T.E. (1973): A low-contamination method for hydrothermal decomposition of zircon and extraction of U and Pb for isotopic age determinations. Geochim. Cosmochim. Acta 37, 495–494.

KROGH, T.E. (1982): Improved accuracy of U–Pb zircon ages by the creation of more concordant systems using the air abrasion technique. Geochim. Cosmochim. Acta 46, 637–649.

LEAKE, B.E. (1978): Nomenclature of amphiboles. Am. Mineral. 63, 1023–1052.

MULCH, A. (1999): Age of synkinematic mafic dikes in the middle and lower crust of the Ivrea-Verbano and Strona-Ceneri Zones (Switzerland and Italy). Unpubl. Diploma thesis, Univ. Giessen, 115 pp.

OPPIZZI, P. and SCHALTEGGER, U. (1998): Zircon-bearing plagioclasites from the Finero complex (Ivrea zone). Dating a Late Triassic mantle hic-cup. Schweiz. Mineral. Petrogr. Mitt. 79, 330–331.

PIDGEON, R.T., NEMCHIN, A.A. and HITCHEN, G.J. (1998): Internal structures of zircons from Archean granites from the Darling Range batholith: implications for zircon stability and the interpetation of zircon U-Pb ages. Contrib. Mineral. Petrol. 132, 288–299.

PIN, C. (1986): Datation U–Pb sur zircons á 285 Ma du complexe gabbro-dioritique du Val Sesia – Val Mastallone et age tardi-hercynien du metamorphisme

granulitique de la zone Ivrea-Verbano (Italie). C.R. Acad. Sci. Paris Sér. II 303, 9, 827–830.

PIN, C. and SILLS, J.D. (1986): Petrogenesis of layered gabbros and ultramafic rocks from Val Sesia, the Ivrea Zone, NW Italy: trace element and isotope geochemistry. In: DAWSON, J.B., CARSWELL, D.A., HALL, J. and WEDEPOHL, K.H. (eds): The Nature of the Lower Continental Crust, Geol. Soc. London Spec. Publ. 24, 231–249.

PINARELLI, L., DELMORO, A. and BORIANI, A. (1988): Rb–Sr Geochronology of Lower Permian plutonism in Massiccio dei Laghi, Southern Alps (NW Italy). Rend. Soc. Ital. Mineral. Petrol. 43, 2, 411–428.

POWELL, R. (1984): Inversion of the assimilation and fractional crystallization (AFC) equations; characterization of contaminants from isotopes and trace element relationships in volcanic suites. J. Geol. Soc. London 141, 447–452.

PUPIN, J. P. (1980): Zircon and granite petrology. Contrib. Mineral. Petrol. 73, 207–220.

RAMSAY, J.G. and HUBER, M.I. (1983): The techniques of modern structural geology. Vol I. Academic Press, London, 307 pp.

ROLLINSON, H. (1993): Using geochemical data: evaluation, presentation, interpretation. Longman Group, UK, London, 352 pp.

SCHALTEGGER, U. (1993): The evolution of the polymetamorphic basement in the Central Alps unravelled by precise U–Pb zircon dating. Contrib. Mineral. Petrol. 113, 466–478.

SCHALTEGGER, U. and BRACK, P. (1999): Short-lived events of extension and volcanism in the Lower Permian of the Southern Alps (Northern Italy, Southern Switzerland). Journal of Conference Abstracts EUG X 4, 1, 296.

SCHMID, S.M. (1993): Ivrea Zone and Adjacent Southern Alpine Basement. In: VON RAUMER, J. F. and NEUBAUER, F. (eds): Pre-Mesozoic geology in the Alps. Springer Verlag, Berlin, 567–583.

SCHMID, S.M., ZINGG, A. and HANDY, M.R. (1987): The kinematics and movements along the Insubric Line and the emplacement of the Ivrea Zone. Tectonophysics 135, 47–66.

SCHNETGER, B. (1994): Partial melting during the evolution of the amphibolite- to granulite-facies gneisses of the Ivrea Zone, northern Italy. Chem. Geol. 113, 71–101.

SCHUMACHER, M.E., SCHÖNBORN, G., BERNOULLI, D. and LAUBSCHER, H.P. (1997): Rifting and collision in the southern Alps. In: PFIFFNER, O.A., LEHNER, P., HEITZMANN, P., MÜLLER, S. and STECK, A. (eds): Deep Structure of the Swiss Alps. Birkhaeuser Verlag, Basel, 186–204.

SHAW, D. M. (1970): Trace element fractionation during anatexis. Geochim. Cosmochim. Acta 34, 239–243.

SINIGOI, S., QUICK, J.E., CLEMENS-KNOTT, D., MAYER, A., DEMARCHI, G., MAZZUCCHELLI, M., NEGRINI, N. and RIVALENTI, G. (1994): Chemical evolution of a large mafic intrusion in the lower crust, Ivrea-Verbano Zone, northern Italy. J. Geophys. Res. 99, B11, 21.575–21.590.

SNOKE, A.W., KALAKAY, T.J., QUICK, J.E. and SINIGOI, S. (1999): Development of a deep-crustal shear zone in response to syntectonic intrusion of mafic magma into the lower crust, Ivrea-Verbano Zone, Italy. Earth Planet. Sci. Lett. 166, 31–45.

STÄHLE, V., FRENZEL, G., KOBER, B., MICHARD, A., PUCHELT, H. and SCHNEIDER, W. (1990): Zircon syenite pegmatites in the Finero peridotite (Ivrea zone): evidence for a syenite from a mantle source. Earth Planet. Sci. Lett. 101, 196–205.

SUN, S.S. (1980): Chemical composition and origin of the earth's primitive mantle. Phil. Trans. Royal Soc. London A297, 409–445.

THOMPSON, R.N. (1982): Magmatism of the British Tertiary Volcanic Province. Scott. J. Geol. 18, 49–107.

TRÜMPY, R. (1992): Ostalpen und Westalpen – Verbindendes und Trennendes. Jb. geol. Bundesanstalt Wien 135(4), 875–882.

TODT, W. (1988): Isotope dilution measurements of Pb, U and Th concentrations in lorandite from Allchar. Nuc. Instr. Meth. Phys. Res. A271, 251–252.

VAVRA, G., GEBAUER, D., SCHMID, R. and COMPSTON, W. (1996): Multiple zircon growth and recrystallization during polyphase Late Carboniferous to Triassic metamorphism in granulites of the Ivrea Zone (Southern Alps): an ion microprobe (SHRIMP) study. Contrib. Mineral. Petrol. 122, 337–358.

VAVRA, G., SCHMID, R. and GEBAUER, D. (1999): Internal morphology, habit and U–Th–Pb microanalysis of amphibolite-to-granulite facies zircons: geochronology of the Ivrea Zone (Southern Alps). Contrib. Mineral. Petrol. 134, 380–404.

VAVRA, G. and SCHALTEGGER, U. (1999): Post-granulite facies monazite growth and rejuvenation during Permian to Lower Jurassic thermal and fluid events in the Ivrea Zone (Southern Alps). Contrib. Mineral. Petrol. 134, 405–414.

VON QUADT, A., FERRARIO, A., DIELLA, V., HANSMANN, W., VAVRA, G. and KÖPPEL, V. (1993): U–Pb ages of zircons from chromitites of the phlogopite peridotite of Finero, Ivrea Zone. N-Italy. Schweiz. Mineral. Petrogr. Mitt. 73, 137–138.

VOSHAGE, H., HOFMANN, A.W., MAZZUCCHELLI, M., RIVALENTI, G., SINIGOI, S., RACZEK, I. and DEMARCHI, G. (1990): Isotopic evidence from the Ivrea Zone for a hybrid lower crust formed by magmatic underplating. Nature 347, 731–736.

WEAVER, B.L., and TARNEY, J. (1981): Lewisian geochemistry and Archean crustal development models. Earth Planet. Sci. Lett. 55, 171–180.

WHALEN, J.B., CURRIE, K.L., and CHAPPEL, B.W. (1987): A-type granites: geochemical characteristics, discrimination and petrogenesis. Contrib. Mineral. Petrol. 95, 407–419.

ZINGG, A. (1983): The Ivrea and Strona-Ceneri Zones (Southern Alps, Ticino and N-Italy) – A review. Schweiz. Mineral. Petrogr. Mitt. 63, 361–392.

ZINGG, A., HANDY, M.R., HUNZIKER, J.C. and SCHMID, S.M. (1990): Tectono-metamorphic history of the Ivrea Zone and its relationship to the crustal evolution of the Southern Alps. Tectonophysics 182, 169–192.

ZULEGER, E. and ERZINGER, J. (1988): Determination of REE and Y in silicate minerals with ICP-AES. Fresenius Z. Anal. Chem., 140–143.

ZURBRIGGEN, R. (1996): Crustal genesis and uplift history of the Strona-Ceneri Zone (Southern Alps). PhD. Thesis, Univ. Bern, 235 pp.

ZURBRIGGEN, R., KAMBER, B.S., HANDY, M.R. and NÄGLER, T.F. (1998): Dating synmagmatic folds: a case study of Schlingen structures in the Strona-Ceneri Zone (Southern Alps, northern Italy). J. Metamorphic Geol. 16, 403–414.

Manuscript received December 18, 2000; revision accepted January 12, 2002.

Appendix

Analytical methods

U–Pb isotopic analyses were carried out on zircon and titanite grains of a hornblende-dioritic enclave in a composite dike and a granite dike. Rock samples were crushed and zircon and titanite grains were separated using standard heavy liquid techniques and a Frantz isodynamic magnetic separator. Preferentially transparent and inclusion-free mineral grains from the 100–160 µm and 160–250 µm sieve fractions were handpicked under a binocular microscope and chosen for analysis. Further selection was based on criteria of morphology and micro-cracking. The zircon grains of the diorite enclave showed a strong response to air-abrasion following the method of KROGH (1982) for 6 hours at 0.6 bars. The grains were briefly washed in 6N HNO_3 on a hot plate, and rinsed several times with distilled water and a mixture of 6N HCI and acetone in an ultrasonic bath. Decomposition was achieved at 180 °C within 60 hours in Teflon-lined stainless steel pressure vessels, using 47% HF as reagent. After splitting and spiking with a $^{208}Pb/^{235}U$ double spike ($^{205}Pb/^{235}U$ spike for zircons of sample MR085) standard chemical procedures for the extraction of U and Pb (KROGH, 1973) were applied. Titanite grains were washed with 3N HNO_3 and rinsed several times with distilled water and acetone. Decomposition was achieved in 47% HF and 13N HNO_3 in

Table A1 Whole rock chemical data of samples from the CMB dike swarm.

Sample	MR081	MR051	MR076	MR079	MR091	MR075	MR 085	MR 165
Rock type	hbl dioritic stock	hbl dioritic dike	hbl dioritic dike	hbl dioritic dike	hbl dioritic enclave	leucosome	granitic dike	granitic dike
SiO_2	45.6	49.7	50.5	49.0	49.3	69.3	71.2	69.4
TiO_2	2.16	1.78	1.40	1.43	1.72	0.40	0.35	0.31
Al_2O_3	17.6	16.5	17.3	15.4	17.3	15.7	15.6	14.7
Fe_2O_3	13.7	11.8	9.72	11.8	10.4	3.21	2.88	3.35
MnO	0.17	0.20	0.17	0.21	0.19	0.06	0.04	0.04
MgO	6.52	6.23	5.93	9.13	4.91	1.04	0.70	0.62
CaO	9.85	10.0	9.57	9.99	9.29	3.54	2.58	2.33
Na_2O	1.57	0.8	2.20	0.7	3.27	4.18	3.55	3.44
K_2O	1.40	0.93	1.27	1.34	1.88	1.27	2.36	2.82
P_2O_5	0.20	0.24	0.25	0.30	0.38	0.17	0.19	0.17
Total	98.77	98.18	98.31	99.30	98.64	98.87	99.45	97.18
Pb /ppm	7	5	9	5	11	17	27	29
Th /ppm	5	5	5	5	9	11	14	17
Rb /ppm	44	35	34	45	53	56	86	102
Sr /ppm	374	352	535	303	570	431	371	295
Y /ppm	42	36	29	35	31	16	14	15
Zr /ppm	73	111	121	110	152	173	225	180
Nb /ppm	8	9	10	8	12	12	13	14
Ba /ppm	300	160	323	193	276	427	897	780
Cr /ppm	50	88	129	378	35	13	10	10
Ni /ppm	10	19	25	82	12	10	10	10
Cu /ppm	44	12	30	21	25	10	10	10
Zn /ppm	100	103	86	94	102	44	62	58
Ga /ppm	19	19	20	15	23	18	19	18
La /ppm	19	16	22	18	25	46	52	49
Ce /ppm	47	35	49	40	58	88	105	103
Pr /ppm	6.7	4.7	6.2	5.7	6.7	8.9	11.8	11.3
Nd /ppm	25	18	22	20	24	26	37	33
Sm /ppm	7.46	5.31	5.75	5.58	5.39	4.20	6.85	6.65
Eu /ppm	1.97	1.64	1.65	1.63	1.64	1.20	1.82	1.35
Gd /ppm	6.06	4.66	4.46	4.97	3.78	2.28	3.6	3.60
Dy /ppm	7.41	6.19	5.10	5.77	4.41	2.68	2.83	2.87
Er /ppm	4.15	3.76	3.03	3.52	2.3	1.65	1.32	1.51
Yb /ppm	3.39	3.07	2.25	2.88	1.88	1.36	0.88	0.90
Lu /ppm	0.56	0.53	0.38	0.49	0.32	0.27	0.17	0.18

closed Savillex beakers on the hot plate for 48 hours. After splitting and spiking with a $^{208}Pb/^{235}U$ double spike a modified procedure of TODT (1988) for the extraction of U and Pb was applied. Total procedural blanks were in the range of 5–8 pg Pb and below 1 pg for U. Pb aliquots were loaded with silica gel and phosphoric acid onto single Re-filaments, U was loaded onto single W-filaments using $TaCl_5$ (zircons of sample MR 085 were loaded on Re-filaments only). Single zircon and titanite isotopic analyses were carried out on a modified Finnigan MAT 261 solid-source mass spectrometer operating in static mode, with ^{204}Pb measured on an ion-counting system. The performance of the detection setup was controlled by additional measurements of NBS 982 standard solution. All errors throughout this publication are given at the 2σ level.

About 10–15 kg of fresh, non-porphyric rock material was sampled for whole rock chemical analysis. Samples from composite dikes were prepared carefully to separate felsic and mafic material. Major and trace elements (except for REE) were determined by X-ray fluorescence (XRF) using a PHILIPS PW 1400 XRF spectrometer. Accuracy and precision were monitored by multiple measurements of international reference standards. REE were determined by inductively coupled plasma-atomic emission spectrometry (ICP-AES) using a PERKIN-ELMER ICP-AES 6000 and following the procedure outlined by ZULEGER and ERZINGER (1988). The full set of geochemical data is given in Table A1. Back-scattered electron (BSE) imaging was performed on a Cameca SX 100 electron microprobe using 20 kV accelerating potential. CL images were obtained from a CamScan SEM at the Université de Lausanne, Switzerland and a Zeiss DSM 962 at the GFZ Potsdam, Germany.

Trace element modelling

Melt Model

To quantify the effects of partial melting on the trace element composition of the melt phase, the equation for non-modal batch melting given by SHAW (1970) is used below. This equation relates the concentration of a trace element in the melt (C_A) to its initial concentration in the non-melted source (C_S):

$$C_A / C_S = 1 / (D_S + F_m (1-D_A))$$

where F_m is the weight fraction of melt produced and D_S is the bulk distribution coefficient for a specific element in the source at the onset of melting. D_S is calculated from

$$D_S = S_i (X_{Si} \times Kd_i)$$

where X_{Si} is the initial mode (weight fraction) of phase i in the source and Kd_i is the mineral-melt-distribution coefficient. D_A is the bulk distribution coefficient for a specific trace element in the partial melt and calculated equally to D_S by substituting X_{Si} with X_{Ai}.

Mineral modes, bulk distribution coefficients, and source rock composition used for the partial melt (PM) calculation are listed in Table A2. Mineral modes and chemistry of the source rock S are consistent with the composition of the IVZ metasediments. Distribution coefficients used for calculation of D_s and D_A are those compiled in ROLLINSON (1993) for granitic compositions.

Assimilation and fractional crystallization (AFC)

According to DEPAOLO (1981) and POWELL (1984), the consequences of assimilation of a crustal component (either bulk rock or anatectic melt) concurrent with fractional crystallization on the trace element composition C of the mantle-derived and crustal-contaminated melt is described by

$$C = C(X_0) \times f + (r/(r-1+D)) \times C(A) \times (1-f)$$

where $C(X_0)$ is the composition of the parental magma, C(A) is the composition of the assimilated contaminant (assimilant) and D is the bulk distribution coefficient of the fractionating crystals (cumulate phases). r is the ratio of the rate of assimilation to the rate of fractional crystallization and ranges between 0 (no assimilation, fractional crystallization only) and 1 (equal amounts of assimilated and crystallized phases). f is calculated from

$$f = F^{-(r-1+D)/(r-1)}$$

where F is the weight fraction of the remaining magma.

Mineral modes, bulk distribution coefficients, parental melt and assimilant compositions used for the calculation and results are listed in Table A2 (AFC and FC stages) for the first stage (r = 0.5) and second stage (r = 0), respectively. X_0 is the mean value of CMB hornblende-diorites, A is the mean value of CMB granites. Distribution coefficients used for the calculation of D are those compiled in ROLLINSON (1993) for basic to intermediate (gabbroic to dioritic) compositions during the first stage and those for intermediate to acid (granodioritic to granitic) compositions during the second stage of AFC.

Table A2 Parameters and results of the partial melt model (PM), the first AFC stage (AFC), and the second FC stage (FC). Abbreviations: S – source, A – assimilant, X_0 – parental magma, D – distribution coefficient, C – element concentration, F_m – extracted melt fraction, F – residual melt fraction.

PM stage						
Modes	**qtz**	**pl**	**bt**	**ms**	**grt**	**zrn**
S	0.44	0.21	0.21	0.1	0.035	0.001
A	0.33	0.33	0	0.33	0	0
D	**S**	**A**		**C**	**S [ppm]**	
Rb	0.96	0.30		Rb	118	
Sr	0.99	1.58		Sr	280	
Nb	0.65	0.02		Nb	13	
Y	1.7	0.03		Y	30	
C/F_m	**ppm/0**	**ppm/0.1**	**ppm/0.2**	**ppm/0.3**		
Rb	123	114	107	101		
Sr	283	301	321	344		
Nb	20	17	15	14		
Y	18	17	16	15		
AFC stage						
D	**0.5hbl 0.5pl**			**C**	**X_0 [ppm]**	**A [ppm]**
Rb	0.045			Rb	42	94
Sr	0.94			Sr	427	333
Nb	0.663			Nb	9	14
Y	1.28			Y	35	15
C/F	**ppm/0**	**ppm/0.1**	**ppm/0.2**	**ppm/0.3**		
Rb	42	57	75	98		
Sr	427	423	418	414		
Nb	9	10	12	13		
Y	35	31	27	24		
FC stage						
D	**0.9pl 0.1ttn**			**C**	**X_1 [ppm]**	
Rb	0.037			Rb	98	
Sr	3.96			Sr	414	
Nb	0.684			Nb	13	
Y	0.09			Y	24	
C/F	**ppm/0**	**ppm/0.2**	**ppm/0.4**	**ppm/0.6**		
Rb	98	121	160	237		
Sr	414	214	91	27		
Nb	13	14	15	17		
Y	24	29	38	55		